UNIVERSITAT DE LES
ILLES BALEARS

Master Thesis

Control of light emission in Parametric Oscillators with Photonic Crystals

Author:
María Moreno de Castro

Supervisor:
Roberta Zambrini

Control of light emission
in Parametric Oscillators
with Photonic Crystals

by

María Moreno de Castro

B.S.(Universidad Autónoma de Madrid) 2006

THESIS

Presented to

Universitat de les Illes Balears

in Partial Fulfillment

of the Requirements

for the Degree of

MASTER OF SCIENCE

September 2009

Acknowledgments

I would like to express my deep-felt gratitude to my supervisor, Roberta Zambrini for her advice, patience and constant support and for giving me the opportunity to begin researching. I also wish to thank the other members of the Instituto de Fisica Interdisciplinar y Sistemas Complejos, specially to the professors of the Master for introducing me the Complex Systems and most of all to Ismael Hernandez, who brought me to Palma, and to the rest of the habitants of the basement. It is really a luck to belong to such a great team. And most, most of all, I am grateful to Alessandro Scire for filling my (scientific) life of surprises.

Finally, I acknowledge the financial support for this work given by the Consejo Superior de Investigaciones Cientificas and, currently, by the Universitat de les Illes Balears. It is a pleasure for me to work as assistant teacher because I learn in the lessons as much as I teach.

Contents

1

Introduction

1.1 Motivation

Since light was quantized by Einstein when studying the photoelectric effect at the beginning of the XXth century, the non classical nature of light, subject of Quantum Optics, has been shown in many different experiments [Bachor & Ralph] and has been involved in the most important fundamental tests of Quantum Physics [Zeilinger]. Moreover, technologies based on quantum phenomena are beginning to enter domains having been dominated by classical optics in two different scenarios. In the first one, a classical technology is pushed until one reaches a point where the operation is limited by quantum noise effects, also due to progressive device miniaturization. In the second scenario, quantum effects allow for novel applications such as quantum communications and, most prominently quantum cryptography. The basis for these innovations is the ability to control and manipulate quantum states of light. This Master thesis is a theoretical work which participates of both perspectives having as objectives the study of quantum fluctuations and fundamental quantum phenomena in optical devices.

Our interest is focused in a non linear optical device, an Optical Parametric Oscillator (OPO), which offers the possibility of quantum phenomena generation and displays a rich spatio-temporal dynamics. When Parametric Down Conversion takes place in this device, the splitting of a beam of frequency ω_p (pump) into two entangled beams of frequency ω_s (signal) and ω_i (idler) occurs due to the quadratic non linearity of the medium. OPOs have become a convenient source of tunable coherent light, especially in the mid-infrared region covering the span of wavelengths from 2 μm to 10 μm, that is often unreachable through other means [Brazhnyi].

Moreover, OPOs have been employed experimentally when testing quantum mechan-

ics, since 'unusual' non classical correlations in the down converted beams were discovered [Burnham & Weinberg] and have become the fundamental tool to achieve insight into quantum optics. Besides, squeezed states (see section 1.3) generated in OPOs are important for technological applications, particularly in the detection of weak signals. A relevant example is the gravitational wave detection with large scale interferometers whose precision will be improved by using squeezed states [Goda].
Until the '90s, **temporal** fluctuations of light beams emerging from non linear devices were mostly investigated, neglecting any spatial effects in the transverse area of the light beam. However, it was realized starting from the seminal paper of [Lugiato & Castelli] that in some cases quantum correlations are present between portions of the beam. On the other hand, it was studied under which conditions quantum properties of the whole beam survive after detection of a part of it [Kolobov]. Following this research line on **spatial** or multimode quantum optics, we include in our model the multimode description of the transverse profile of a light beam emerging from an OPO. Interference between off-axis down converted beams causes, for large Fresnel numbers, not only spatio-temporal instabilities but also quantum correlations. In particular, in the last decade, several quantum and classical phenomena have been studied in multimode OPOs.
Here we propose to investigate a prototype system, that is the Degenerate Optical Parametric Oscillator embedding a Photonic Crystal (PCOPO), in order to analyze if the photonic crystal improves OPO performance. The use of photonic crystals in non linear devices was first proposed by [Gomila & al. (03)] and two recent experiments [Terhalle & al.], [Marsal & al.] have confirmed those theoretical predictions, as we will explain in Chapter 3.
In the following we will introduce the main subjects of interest in this project, starting from the devices we will consider, namely OPOs and photonic crystals. Later we will give a brief overview of spontaneous pattern formation followed by an introduction about the quantum phenomena we analyze in our study.

1.2 Physical Systems

1.2.1 Optical Parametric Oscillator (OPO)

An Optical Parametric Oscillator (OPO) is a cavity containing a quadratic crystal. The non linear process taking place is the Parametric Down Conversion, described in the following.
Parametric Down Conversion is a wave-mixing process in which the pump decays into

two beams at lower frequencies, historically called signal and idler. Energy (given in terms of the frequency $E = \hbar\omega$) and momentum (given in terms of the wavenumber $\vec{p} = \hbar\vec{k}$) are preserved, as it is expressed in the phase matching conditions:

$$\omega_p = \omega_s + \omega_i; \qquad \vec{k}_p = \vec{k}_s + \vec{k}_i \tag{1.1}$$

The special case we deal with is called Degenerate Parametric Down Conversion being $\omega_s = \omega_i \equiv \omega$.

The Hamiltonian of this process expressed in terms of the creation operators $\hat{a}^\dagger, \hat{b}^\dagger$, at frequency ω and ω_p respectively, and the corresponding annihilation operators $\hat{a}, \hat{b}$, is [Gerry]:

$$\hat{H} = \hbar\omega\hat{a}^\dagger\hat{a} + \hbar\omega_p\hat{b}^\dagger\hat{b} + i\hbar\chi^{(2)}(\hat{a}^2\hat{b}^\dagger - \hat{a}^{\dagger 2}\hat{b}). \tag{1.2}$$

The second-order susceptibility $\chi^{(2)}$ characterizes the 'quadratic' medium, when, as usually, the response is given in terms of the polarization:

$$p(t) = \chi^{(1)}E(t) + \chi^{(2)}E(t) : E(t) + \chi^{(3)}E(t) : E(t) : E(t) + ... \tag{1.3}$$

We assume the simplest case, i.e. lossless and dispersionless media, for which the response is instantaneous [Boyd]. $\chi^{(2)}$ is different from zero only in noncentrosymmetric crystals, where there is not inversion symmetry, so the material must be anisotropic. The most commonly used crystals are KDP (KD_2PO_4) and BBO ($\beta - BaB_2O_4$). When the material has not a preferred direction, for example a gas, $\chi^{(2)}$ vanishes and the third-order susceptibility is the important coefficient (as in Kerr media). In the case of low power pump, only the linear polarization is taken into account.

Within the 'parametric approximation' the injected intense laser is assumed to remain undepleted at relevant time scale. Such intense kind of light is well described by coherent states (see section 1.3) which, in the Schödinger picture, evolve in time as harmonic oscillators. Then we can approximate the pump annihilation and creation operators $\hat{b}(t)$ and $\hat{b}^\dagger(t)$ by $\beta e^{-i\omega_p t}$ and $\beta^* e^{i\omega_p t}$, respectively, and, within the Heisenberg picture, with operators time-evolution given by $\hat{a}(t) = \hat{a}(0)e^{-i\omega t}$, the interaction part of the Hamiltonian yields:

$$\hat{H}_I = i\hbar\chi^{(2)}(\beta^*\hat{a}^2 e^{i(\omega_p - 2\omega)t} - \beta\hat{a}^{\dagger 2}e^{-i(\omega_p - 2\omega)t}) \tag{1.4}$$

Considering the degenerate relation between frequencies: $\omega_p = 2\omega$ we obtain:

$$\hat{H}_I = i\hbar\chi^{(2)}(\beta^*\hat{a}^2 - \beta\hat{a}^{\dagger 2}). \tag{1.5}$$

which is the simplified interaction Hamiltonian for the Degenerate Parametric Down Conversion process we will consider in Chapter 2.

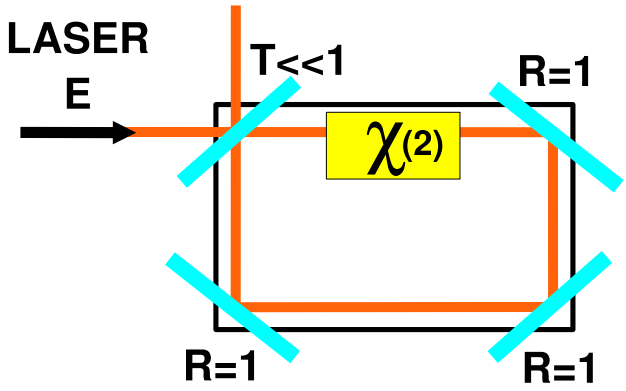

Figure 1.1. Optical Parametric Oscillator scheme. An incoming coherent laser beam E is injected into the cavity containing a quadratic crystal ($\chi^{(2)}$). Three mirrors have total reflectivity R while input and output beams pass through the mirror with non null transmittivy T.

As we mentioned, we consider the process of Parametric Down Conversion enhanced by an optical cavity that is a **Optical Parametric Oscillator**. Resonant cavities act as optical amplifiers that highly improves the efficiency of wave-mixing processes as Parametric Down Conversion when the natural frequency is near to ω_s, ω_i or both. For pump intensity high enough to make second-order polarization important and to balance the losses experienced at each round-trip, the non linear system reaches its threshold for down conversion. Losses are due to outcoupling by one of the resonator mirrors (with $T << 1$), which provides the desired output wave. The scheme of an Optical Parametric Oscillator (OPO) is given in Fig.1.1.

OPOs share many features with lasers, yet there exists a important difference between them. Unlike lasers, which rely on population inversion in a gain material in the required wavelength range, OPOs exploit optical frequency conversion in a non linear crystal with a non resonant interaction (no population inversion, passive optical devices). Over the years, OPOs have become the key element for the production of squeezed states and the realization of fundamental quantum optics experiments with new records of squeezing almost achieving the maximum possible value [Vahlbruch & al.]. From the technological point of view, OPOs are still subject of investigation in relation to their stability under temperature changes [Canalias& Pasiskevicius] or to their performance without mirrors [Khurgin].

Process of Parametric Down Conversion can be phase-matched in two different ways. This gives rise to parametric oscillators of type I or type II depending on the polarization of the down converted fields, as represented in Fig 1.2. This is a consequence of birefringence, i.e. the dependence on the direction of polarization of the index of refraction. Materials

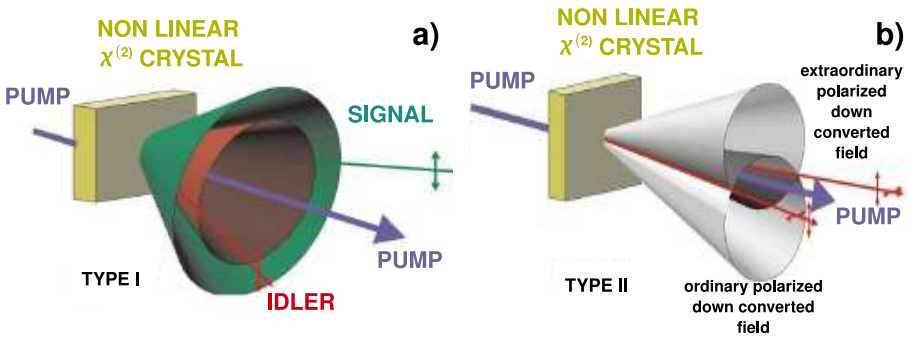

Figure 1.2. a) Type I Parametric Down Conversion. Photons from the pump beam are converted into signal and idler photons that emerge from the non linear crystal. The down converted fields have identical polarizations but orthogonal to the pump. In our case, as we deal with a type I degenerated OPO, both signal and idler are at the same frequency. b) Type II Parametric Down Conversion. The signal and the idler photons have orthogonal polarizations. Light in the intersections of the cones for the extraordinary polarized beam and the ordinary one is in polarization entangled state. (From ftp://ftp.cordis.europa.eu/pub/ist/docs/fet/qip2-eu-08.pdf).

displaying birefringence are phase-matchable [Boyd]. Then, two beams emerge linearly polarized in different directions, the *ordinary* one, seeing a refractive index $n = n_o$ and the *extraordinary* one, seeing a refractive index $n = n_e/\beta(\theta)$, where θ is the angle of incidence [Hecht]. As we choose to work in a *positive* (i.e. $n_e > n_o$) and *type I* crystal (i.e. the lower-frequency waves have the same polarization), the pump will be ordinary polarized and signal and idler will be extraordinary polarized [Boyd].

1.2.2 Photonic Crystals

Photonic crystals (PC) consist of regularly alternate regions of high and low dielectric constant ϵ or refractive index ($n \sim \sqrt{\epsilon}$ for most optical porpoises). Due to their periodicity, photonic crystals display peculiar propagation properties.

Let us consider a periodic modulation of the refractive index with lattice constant a (Fig. 1.4a), and a propagating plane wave of wavelength λ. For λ of the same order of a, the multiple reflections from the lattice causes light to interfere. Indeed, for $\lambda = 2a$ the multiple reflections from the scattering center cancel out, preventing light from propagating into the medium. The continuous translational symmetry characteristic of a uniform media is broken and becomes discrete. As usually, a symmetry breaking destroys a degeneracy. In fact, the mode:

$$k = \frac{2\pi}{\lambda}|_{\lambda=2a} = \frac{\pi}{a} \tag{1.6}$$

in a uniform medium would have frequency equal $\omega = kc/n$, but in a photonic crystal of lattice constant a it splits in two frequencies $\omega(n_1)$ and $\omega(n_2)$, one having its maximum in the n_1 region and its nodes in the n_2 region and other having its maximum in the n_1 region and its nodes in the n_2 region. In terms of the energy it can be proved [Joannopoulos & al.] that the low-frequency modes concentrate their energy in the high-ϵ regions, and the high-frequency modes have a larger fraction of their energy (although not necessarily a majority) in the low-ϵ regions. This is the physical reason of the discontinuity at $k = \pi/a$ in the dispersion diagram, called **band gap** (Fig. 1.4b).

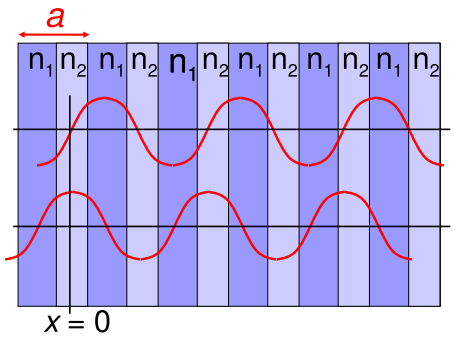

Figure 1.3. Periodically modulated medium, with periodicity a and two different refractive index n_1 and n_2 where $n(x) = n(x + a)$. Two waves propagating within the medium with $\lambda = 2a$ and a relative phase equals π see the two refraction index separately, i.e. the upper one having its nodes in the n_2 zone has always a frequency equals $\omega_1 = kc/n_1$ when in the same region the lower wave has its maximum thus always propagates at $\omega_2 = kc/n_2$. For wavelengths submultiples, fulfilling $\lambda = 2a/n$ ($n = \{2, 4, ..\}$) there is also band gap. However, its width decreases as n increases because the relative difference between nodes and maxim values becomes neglectable. For $\lambda = 2an$ ($n = \{2, 4, ..\}$) instead, there is not band gap because the photonic crystal can be considered as homogeneous.

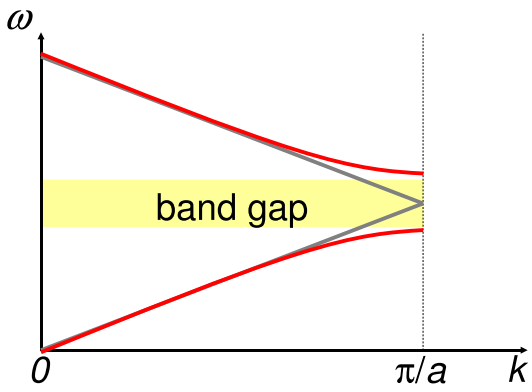

Figure 1.4. Dispersion diagram for a uniform medium where an arbitrary periodicity with a lattice constant has been chosen (in grey) and for a periodically modulated medium with lattice constant a (in red) for the first irreducible Brillouin zone. For uniform media, the refraction index is a constant thus $\omega = \frac{ck}{n}$ gives a straight line and for periodically modulated media angular frequency becomes discontinuous at $\lambda = 2a$. Therefore, no wave propagate at those frequencies. The larger the difference between the refractive indexes the wider the band gap.

Therefore, photonic crystals prevent the propagation of a range of frequencies, as semiconductors prevent electrons from passing through. Band gaps always appear in a one-dimensional photonic crystal for any refractive index contrast. The larger the contrast, the larger the gaps.

It is possible to create energy levels in the photonic band gap by defecting the material. This is the photonic equivalent to breaking the perfect periodicity of semiconductor lattice. This has given rise distint optical phenomena like omni-directional high-reflectivity and low-loss-waveguiding, amongst others, related to the control of the flow of light. This

topic has increasing interest owing to the current explosion in optics communication and information technology.

The construction of a three-dimensional photonic crystal with a complete photonic bandgap in the optical wavelength region has been a challenge. In this case the periodicity of the photonic crystal structure has to be of the same length-scale as half the wavelength of the electromagnetic waves, meaning from 200 nm (blue) to 350 nm (red). Therefore the fabrication of photonic crystals is cumbersome and complex, although there are various important achievements [Sun], [Blanco & al.], [Noda & al], mostly using semiconductors as GaAs, the best material for integration into optoelectronic devices [Yablonovitch (00)]. In our work we focus on the effect of photonic crystals to control light emission as it will be shown in Chapters 3 and 4, respectively, rather than in the characterization of specific technical features of photonic crystals. Our theoretical model includes a one-dimension photonic crystal as a medium with modulated refractive index:

$$n = \eta \sin(k_{pc} x) \tag{1.7}$$

being x orthogonal to the propagation axes. In other words, we will modulate the **transverse** profile of the light beam.

Photonic crystals had been studied since long time ago. Lord Rayleigh in the 19th century showed that such systems have a one-dimensional photonic band-gap, known as a stop-band, a spectral range of large reflectivity when driving a beam in a certain angle to a surface (Bragg mirror). One hundred years later the name 'photonic crystal' appeared for first time in [Yablonovitch (87)], [John] simultaneously. The main motivation of the first work was to engineer the photonic density of states, in order to control the spontaneous emission of materials embedded within the photonic crystal, while the idea contained in the second one was to use photonic crystals to affect the localization and control of light.

1.3 Phenomena

The question we address in this Master thesis is wether the implementation of an intracavity photonic crystal affects the non linear and quantum phenomena occurring in OPOs. We will then introduce Pattern Formation in the context of optics, as a non linear phenomena arising in complex systems. Then we will define the quantum phenomena we are interested, which are the Spatial Antibunching and the Quadrature Squeezing.

1.3.1 Pattern Formation

From the stripes of a zebra to a desert dune, regular patterns arise everywhere in nature. Of course, there is an element of subjectivity in perceiving patterns. A pattern might be regarded as a regularly repeating array of identical units. For a more open definition one can include arrays of units that are similar but not necessary identical, and which can repeat but not necessarily regularly or with a well-defined symmetry [Ball].
The appearance and evolution of patterns have been a focus of research activity across several disciplines. In fact, in spite of the variety of systems in which patterns appear, there is a fundamental universal character, allowing for a unified approach to the problem. Characteristics such as the number of degrees of freedom, symmetries, the type of non linearity and of coupling terms (gradients, diffusion, diffraction...) overcome the importance of the specificity of the optical, chemical, acoustical or fluid system.
Spontaneous pattern formation phenomena are characterized by the existence of instabilities in certain quantity arising when the system is brought sufficiently away from thermal equilibrium by increasing a control parameter [Cross & Hohenberg]. In other words, the phenomenon does have a threshold.
Pattern formation in optics was predicted in 1987 by [Lugiato & Lefever]. Since then, many theoretical studies and experimental realizations (see Fig. 1.5) have been reported in this area. We will focus in the transverse profile multimode interference. Optical pattern formation is found pumping non linear devices with large Fresnel number and allowing for losses. In our system, the spatial communication between different parts of the beam in order to be coupled is achieved by diffraction and there is an additional condition over the signal detuning (it must be negative), derived in Chapter 3.

In Fig. 1.7 we show with a numerical simulation the optical pattern created by an OPO above threshold in the transverse profile of the outgoing beam, in comparison to what happens below threshold, Fig. 1.6. The spatial modes composing the pattern can be visualized in the far field which is the Fourier transform of the near field. Precisely, the

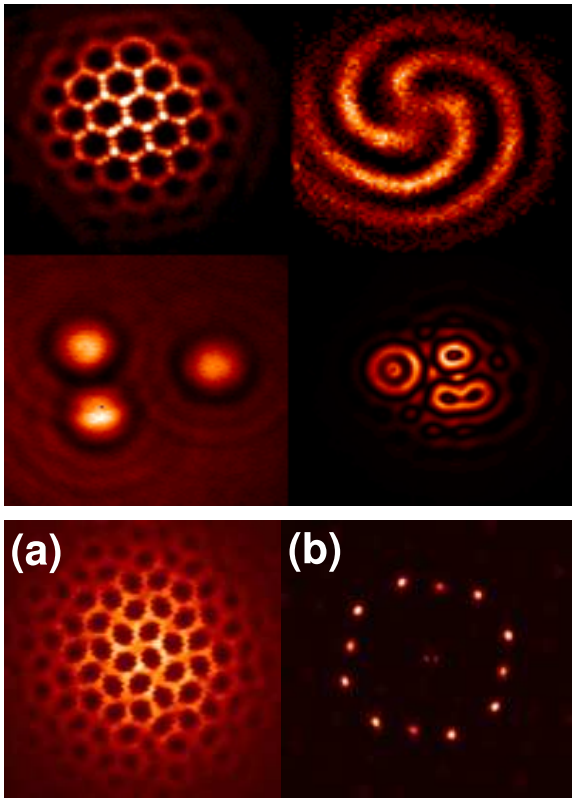

Figure 1.5. The first four panels show examples of two dimensional optical patterns in a laser beam obtained in an experiment with alkali metal vapors as non linear media (χ^3), and a feeback mirror. It is worth to remark that it is not a structure formed by the molecules of the gas, but the transverse profile of the outgoing light. Picture (b) corresponds to the pattern showed in (a) as observed in the far field, which is obtained with a lens and corresponds to the Fourier transform of the near field. (From http://www.photonics.phys.strath.ac.uk/NonlinearPhotonics/na.html)

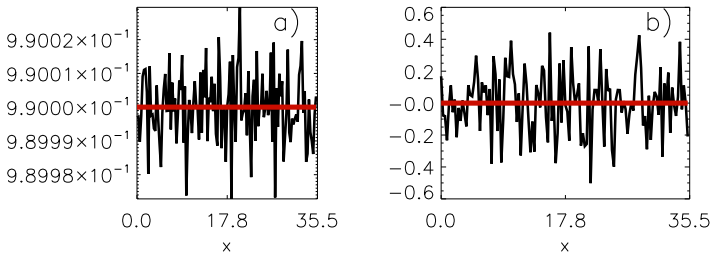

Figure 1.6. Real part of pump (a) and signal (b) fields generated by numerical simulation of a Type I Degenerate Optical Parametric Oscillator without photonic crystal, 1% below threshold, in agreement with the theoretically predicted value given in Eq. (2.41) for the steady state in the case of pump detuning equal zero (see Chapter 2). In black it is plotted the noisy initial condition and in red, the transverse profile of the fields after temporal transients. The noise amplitude for the pump is 0.001 while the one for the signal is 0.2. As the pump is below threshold, the output at frequency 2ω remains in the value provided by the injected laser beam (a) while the signal at frequency ω field just switches off (b). Imaginary parts of both fields also vanish.

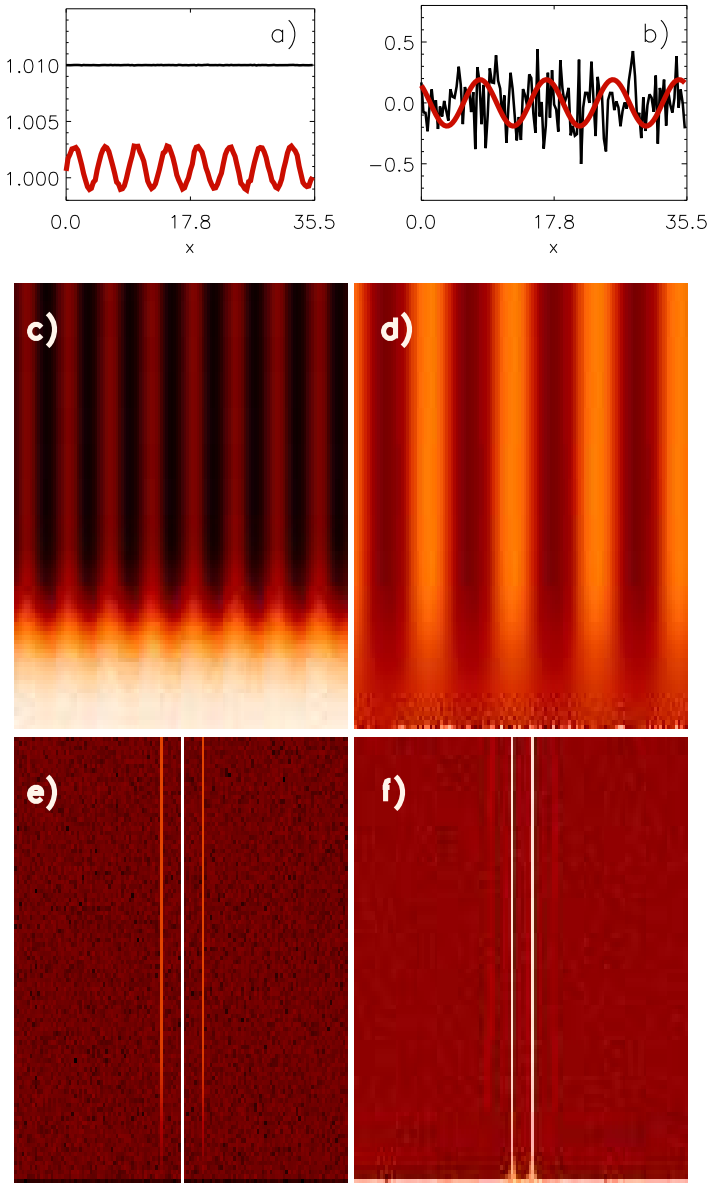

Figure 1.7. Real part of pump (a) and signal (b) fields generated by numerical simulation of a Type I Degenerate Optical Parametric Oscillator without photonic crystal 1% above its threshold. In black the fields are plotted at $t = 0$ (noisy initial condition with amplitude for the pump equal 0.001 and for the signal 0.2) and in red they are plotted after transient evolution. In pictures c) and d) the horizontal axes is x (real space or near field) and the vertical one is time. After a transient state, a stripe pattern is formed in both fields. In the pump near field (c) we observe a pattern with twice the wavelength of the pattern in the signal (d) owing to the phase matching conditions for the Parametric Down Conversion, Eq. (1.1). Pictures e) and f) show the far field, i.e. the Fourier transform of the near field given in c) and d), here in logarithm scale. Thus, the horizontal axes is k_x and the vertical one is time. Far fields for a fixed time show a spot for the homogeneous pump ($k = 0$) and two spots at $k = \pm 2k_c$, while there are two spots for the signal at $k = \pm k_c$. The simulations are performed with periodical boundary conditions. Imaginary parts of both fields at final t are zero.

pattern is given by a linear combination of plane waves $\exp(ik_x x)$, where x is the position for one transverse dimension considered here and k_x is the wave vector. For our purposes it will be enough to consider the case of one transverse dimension, as it can be obtained by imposing a waveguide configuration. This leads to the formation of only stripe patterns (in the near field). In the far field, in first approximation valid near threshold, this stripe pattern corresponds to a 3-spot structure [Lugiato, Lugiato & al. (95)], in which the central spot arises from the axial pump beams, while the other two spots arise from signal beams with transverse non-vanishing wavevectors, $+k$ and $-k$, generated by the spatial instability and propagating symmetrically with respect to the axis of the system (Fig. 1.7). The wave-number k is linearly selected at threshold (see Chapter 3), but the shape of the spatial structure is determined by a non linear selection process [Cross & Hohenberg]. In two dimensions this can give rise to hexagons [Grynberg & al.], [Grynberg & Lugiato], squares, quasipatterns, ...

The pattern our devices creates in the transverse profile of the signal outgoing beam are stripes with a critical wave number k_c. In order to control such spatial instabilities we focus our study in the case where the photonic crystal modulation wavenumber, introduced in Eq. 1.7, and the critical one are commensurable. The maximun effect of the photonic crystal in terms of band gap creation occurs for k transverse momentum such that:

$$k_{pc} = 2k. \tag{1.8}$$

With this relation in mind we will study the role of a photonic crystal on the instabilities in a OPO in Chapter 4.

1.3.2 Quantum Phenomena

Quantum phenomena we are interested in are spatial antibunching and squeezing, and in this section we will introduce them. We have to emphasize the fact that all the states of light share quantum nature due to the discreteness of the photons. In practice however non classical properties of light are difficult to observe and only with the development of lasers, the study of quantum optics started, half a century ago.

First order coherence

Photon antibunching is significant for the quantum theory of light, as it cannot occur neither in the classical nor in the semiclassical theory and its treatment requires the quantum photocount theory. We first start with the classical detection of optical fields. Considering a scalar classical electromagnetic field in a detector, as the superposition of two

waves following the path s_1 and s_2 respectively, thus the path difference is $\Delta s = |\vec{r}_1 - \vec{r}_2|$ (as in the Young's double split). The averaged intensity of light at the detector contains the crossing term $2Re\langle E^*(\vec{r}_1, t_1)E(\vec{r}_2, t_2)\rangle$ related to the interference, one of the most important features of light considered as a wave. Averages are considered in an ensemble and in most of the cases this is equivalent to perform temporal averages. The first-order normalized mutual coherence function is defined as:

$$g^{(1)}_{class}(\vec{r}_1, t_1; \vec{r}_2, t_2) = \frac{\langle E^*(\vec{r}_1, t_1)E(\vec{r}_2, t_2)\rangle}{\sqrt{\langle |E^(\vec{r}_1, t_1)|^2\rangle \langle |E(\vec{r}_2, t_2)|^2\rangle}}. \tag{1.9}$$

Depending on the values of this function we have different degrees of first order coherence as summarized below:

$$\vec{r}_1, \vec{r}_2, t_1, t_2 \text{ such that } \begin{cases} |g^{(1)}_{class}| = 1 \rightarrow \textit{complete coherence} \\ 0 < |g^{(1)}_{class}| < 1 \rightarrow \textit{partial coherence} \\ |g^{(1)}_{class}| = 0 \rightarrow \textit{complete incoherence.} \end{cases} \tag{1.10}$$

Physically, when a source has a bandwidth of $\Delta\omega$, interference will occur if $\Delta s \leq \frac{c}{\Delta\omega}$ and the quantity $\Delta s_{coh} = \frac{c}{\Delta\omega}$ is called the coherence length with the corresponding coherence time $\Delta\tau_c = \Delta s_{coh}/c = 1/\Delta\omega$. In other words, for $|t_1 - t_2| < \Delta\tau_c$ $g^{(1)}_{class} > 0$. From the conditions exposed in Eq. (1.9) one can analyze both the spatial and the temporal coherence of a given light beam by calculating the corresponding, spatial or temporal, first-order coherence function. For example, when we are interested in a monochromatic light field propagating in the z direction at position z and times t ant $t+\tau$, we calculate the autocorrelation function $\langle E^*(z,t)E(z,t+\tau\rangle$ and we obtain $g^{(1)}_{class}(z,z,t,t+\tau) = g^{(1)}_{class}(\tau) = e^{-i\omega\tau}$. Therefore $|g^{(1)}_{class}(\tau)| = 1$ and, as we expect, we have complete temporal coherence for any τ.

The quantum analogous of the first-order degree of coherence criterion, given in Eq. (1.9), is obtained from the expectation value of a product of field operators. In the following we introduce its physical meaning within the theory of quantum photodetection. The intensity of a beam is measured by the absorption of the photons in a medium, whose ionization response is electrically detected. An ideal detector consists of a single atom of dimension small compared to the wavelength of the light, i.e. it holds the dipolar approximation ($|\vec{k}\cdot\vec{r}| << 1$). The single-atom detector couples to the scalar quantized field, in the direction given for the unitary vector $\vec{u}_{\vec{k}}$ [Loudon]:

$$\hat{\vec{E}}(\vec{r}, t) \propto i\sum_{\vec{k}} \sqrt{\hbar\omega_k}\vec{u}_{\vec{k}}(\hat{a}_k e^{i(\vec{k}\cdot\vec{r}-\omega_k t)} - \hat{a}^\dagger_k e^{-i(\vec{k}\cdot\vec{r}-\omega_k t)}) \approx i\sum_{\vec{k}} \sqrt{\hbar\omega_k}\vec{u}_{\vec{k}}(\hat{a}_k e^{i(\omega_k t)} - \hat{a}^\dagger_k e^{-i(\omega_k t)}) \tag{1.11}$$

through the dipole interaction:

$$\hat{H}_d = -\hat{d}\hat{E} \tag{1.12}$$

where $\hat{d}$ is the dipole moment operator. Absorption of a photon in the detector (named 'ab') is proportional to the annihilation operator, termed $\hat{E}^{(ab)}$ while the emission ('em') corresponds to the creation operator part, termed $\hat{E}^{(em)}$, where $\hat{E}^{(em)} = (E^{(ab)})^{\dagger}$, so we rewrite:

$$\hat{\vec{E}}(t) = \hat{\vec{E}}(t)^{(ab)} + \hat{\vec{E}}(t)^{(em)} \tag{1.13}$$

The probability that the field undergoes a transition form an initial state $|i\rangle$ to a final state $|f\rangle$ is proportional to $|\langle f|\hat{E}^{(ab)}|i\rangle|^2$ for a pure state. We are interested in the final state of the detector thus we sum over all possible final states (reminding Fermi's Golden Rule):

$$\sum_f |\langle f|\hat{E}^{(ab)}|i\rangle|^2 = \sum_f \langle i|\hat{E}^{(em)}|f\rangle\langle f|\hat{E}^{(ab)}|i\rangle = \langle i|\hat{E}^{(em)}\hat{E}^{(ab)}|i\rangle \tag{1.14}$$

considering $\{|f\rangle\}$ as a complete set. For a mixed state described by a density operator of the form $\hat{\rho} = \sum_i P_i|i\rangle\langle i|$, this expectation value is replaced by the ensemble average, given by the trace over initial states, named:

$$G^{(1)} = Tr(\hat{\rho}\hat{E}^{(em)}\hat{E}^{(ab)}). \tag{1.15}$$

related to the number operator expection value. As in general, we are analyzing the superposition of the fields with different path lengths. Then:

$$G^{(1)}(\vec{r}_1, t_1; \vec{r}_2, t_2) = Tr(\hat{\rho}\hat{E}^{(em)}(\vec{r}_1, t_1)\hat{E}^{(ab)}(\vec{r}_2, t_2)). \tag{1.16}$$

The intensity of the light in the photo-detector depends on $G^{(1)}(\vec{r}_1, t_1; \vec{r}_1, t_1)$ and $G^{(1)}(\vec{r}_2, t_2; \vec{r}_2, t_2)$ and on a crossing term $G^{(1)}(\vec{r}_1, t_1; \vec{r}_2, t_2)$ which is a measure of interference. The normalized first-order quantum coherence function analogous to Eq.1.9 is:

$$g^{(1)}(\vec{r}_1, t_1; \vec{r}_2, t_2) = \frac{G^{(1)}(\vec{r}_1, t_1; \vec{r}_2, t_2)}{\sqrt{G^{(1)}(\vec{r}_1, t_1; \vec{r}_1, t_1)G^{(1)}(\vec{r}_2, t_2; \vec{r}_2, t_2)}} \tag{1.17}$$

discerning the three spatio-temporal intervals of coherence as in the classical case, Eq.1.10.

Second Order Coherence and Antibunching

First order coherence function is appropriated to determine the degree to which a light source is monochromatic because is related to interference due to phase difference but it says nothing about the statistical properties of the light. First-order coherence experiments (as Young's double slit) are unable to distinguish between light beams with identical spectral distributions but in quite different states. Another kind of interferometry experiment is necessary in order to characterize the quantum states of light. The measured

quantities are now intensities instead of fields and the detector measures the number of coincidences in the arrival of photons coming from the same source [Hanbury Brown & Twiss]. Let us consider a detector registering up a count at time t and also at $t+\tau$. If the delay time τ is smaller that the coherence time $\tau_c = 1/\Delta\omega$, information on the statistics of the splitted light can be extracted.

Starting with the classical approach, the rate coincident counts should be proportional to the two times intensity correlation, $\langle I(t)I(t+\tau)\rangle$. If the average of the intensity at each detector is $\langle I(t)\rangle$, then the probability of obtaining a coincidence count with time delay τ is named the classical second-order coherence function:

$$g^{(2)}_{class}(t,t+\tau) = \frac{\langle I(t)I(t+\tau\rangle}{\langle I(t)\rangle\langle I(t+\tau)\rangle}. \tag{1.18}$$

We have seen that the magnitude of the degree of first order coherence takes values in the range 0 to 1. The allowed range of values of the degree of second order coherence is controlled by Cauchy's inequality, which applies to any pair of real numbers. Thus two measurements of the intensity at times t_1 and t_2 must satisfy:

$$2I(t_1)I(t_2) \leq I(t_1)^2 + I(t_2)^2. \tag{1.19}$$

If we now consider the average $\langle\ \rangle$ taken over N measurements, by applying this inequality to the cross terms, it is easy to show that:

$$\left(\frac{I(t_1)+I(t_2)+...+I(t_N)}{N}\right)^2 \leqslant \frac{I^2(t_1)+I^2(t_2)+...+I^2(t_N)}{N} \tag{1.20}$$

Thus:

$$\langle I(t)\rangle^2 \leq \langle I^2(t)\rangle \tag{1.21}$$

and the degree of second order coherence for zero time delay form Eq. (1.18) satisfies:

$$1 \leq g^{(2)}(0). \tag{1.22}$$

It is not possible to establish any upper limit, and the complete range of allowed values is:

$$1 \leq g^{(2)}(0) \leq \infty. \tag{1.23}$$

Our definition 1.18 assumes a stationary light beam (i.e. only dependent on time delay τ) but they also apply to a series of measurements on nonstationary light. For the extreme example of a single optical pulse, it is clear that measurements at a fixed observation point must produce quite different results that depends on the locations of the pulse at

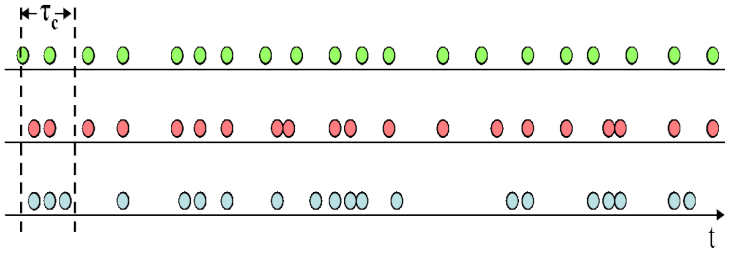

Figure 1.8. First line: photons arrive spaced in time for the quantum effect of temporal anti-bunching ($g^{(2)}(\tau) > g^{(2)}(0)$), as in the single-mode field. Second line: photons arrive randomly in time independent complete coherence ($g^{(2)}(\tau) = g^{(2)}(0) = 1$), as in quantum coherent states. Third line: photons arrive bunched in the classical effect of temporal bunching ($g^{(2)}(\tau) < g^{(2)}(0)$), as thermal (or chaotic) states of light. The statistical properties will be analyzed in the following section. The coherence time of the emitted light, inversely proportional to the spectral width of the source, $\tau_c = 1/\Delta\omega$, is also represented. (Courtesy of $http://en.wikipedia.org/wiki/Degree\_of\_coherence$)

the times of measurements. There is not equivalence between time and statistical averaging in this case. However, the N measurements of the intensity envisaged in Eq. (1.20) can in principle be made at the same time but on members of an ensemble of N realizations of the same optical pulse. The inequalities in Eqs. (1.22) and (1.23) continue to apply with this interpretation of the averaging, and they can be taken as general properties of all kinds of classical light.

The above proof cannot be extended to nonzero time delays, and the only restriction on the degree of second order coherence then results from the essentially positive nature of the intensity, which gives

$$0 \leq g^{(2)}(\tau) \leq \infty \quad \tau \neq 0. \tag{1.24}$$

There is, however, another important property that follows from the inequality

$$((I(t_1)I(t_1+\tau)+...+I(t_N)I(t_N+\tau))^2 \leq (I(t_1)^2+...+I(t_N)^2)(I(t_1+\tau)^2+...+I(t_N+\tau)^2) \tag{1.25}$$

which is also established with the use of Cauchy's inequality Eq. (1.19). The two summations on the right are equal for sufficiently long and numerous series of measurements, and the squared root of Eq. (1.25) then produces the result:

$$\langle I(t)I(t+\tau)\rangle \leq \langle I^2(t)\rangle \rightarrow g^{(2)}_{class}(\tau) \leq g^{(2)}(0). \tag{1.26}$$

If light incident on one of the detectors is independent of the light incident on the other, there should be a uniform coincidence rate independent of t. For a source of thermal light (also known as chaotic light which follows the Planck's statistic distribution for the blackbody radiation), at zero time delay it is found twice the detection rate compared with the rate at long time delays. This means that

$$g^{(2)}(0) \sim 2g^{(2)}(\infty) \tag{1.27}$$

i.e, photons arrive in pairs at zero time delay but independently at long time delays (when generally $g^{(2)}(\infty)$ 1 as shown in the third line in Fig. 1.8). That photons arrive in 'bunched' pairs is known as *photon bunching* or the Hanbury Brown and Twiss effect [Hanbury Brown & Twiss].

When focusing in the quantum derivation of the second-coherence function it will become clear that there are instances where the predictions from quantum theory do not have classical counterpart. Following the steps given for the first-order quantum coherence, the transition probability for the absorption of two photons is proportional to

$$|\langle f|\hat{E}^{(ab)}(\vec{r}_2,t_2)E^{(ab)}(\vec{r}_1,t_1)|i\rangle|^2. \tag{1.28}$$

After summation over all final states and generalizing to cases of nonpure field, the ensemble average of $I(\vec{r}_1,t_1)I(\vec{r}_2,t_2)$ is:

$$G^{(2)}(\vec{r}_1,t_1;\vec{r}_2,t_2) = Tr(\hat{\rho}\hat{E}^{(em)}(\vec{r}_1,t_1)\hat{E}^{(em)}(\vec{r}_2,t_2)\hat{E}^{(ab)}(\vec{r}_2,t_2)\hat{E}^{(ab)}(\vec{r}_1,t_1)) \tag{1.29}$$

and the second-order quantum coherence function is expressed as:

$$g^{(2)} = \frac{G^{(2)}(\vec{r}_1,t_1,\vec{r}_2,t_2;\vec{r}_2,t_2,\vec{r}_1,t_1)}{G^{(2)}(\vec{r}_1,t_1,\vec{r}_1,t_1)G^{(2)}(\vec{r}_2,t_2,\vec{r}_2,t_2)} \tag{1.30}$$

which is the joint probability of detecting one photon at $\vec{r}_1$ at time t_1 and a second at $\vec{r}_2$ at time t_2. When $g^{(2)} = 1$ the probability of a delayed or shifted in space coincidence is independent of either time or space respectively, so as we said before, the detection in one screen is independent of the detection in the other screen. A quantum field is second-order coherent if both, first and second order coherence function equals unity. For the case of time coherence we fix position ($r_1 = r_2$) and for stationary states $g^{(2)}$ only depends on τ. Then:

$$g^{(2)}_{class}(\tau) < g^{(2)}_{class}(0) \tag{1.31}$$

characterizes photon bunching, a property exhibited by thermal light, as we explained before. Eq. (1.31) means that correlations between separated events are smaller than correlations of an event with itself. Then, correlations of separated events decay with time separation as generally found within classical optics. The left panel in Fig. 1.9 shows experimental results when measuring photon bunching at ultrashort timescale by two-photon absorption in semiconductors [Boitier & al.]. Second-order coherence for blackbody radiation (thermal or chaotic light with $g^{(2)}(\tau) < g^{(2)}(0)$) is compared with the one measured for a laser beam (coherent light with $g^{(2)}(\tau) = 1$).

Nevertheless, some quantum states of light violate the inequality of Eq. 1.31 given rise to

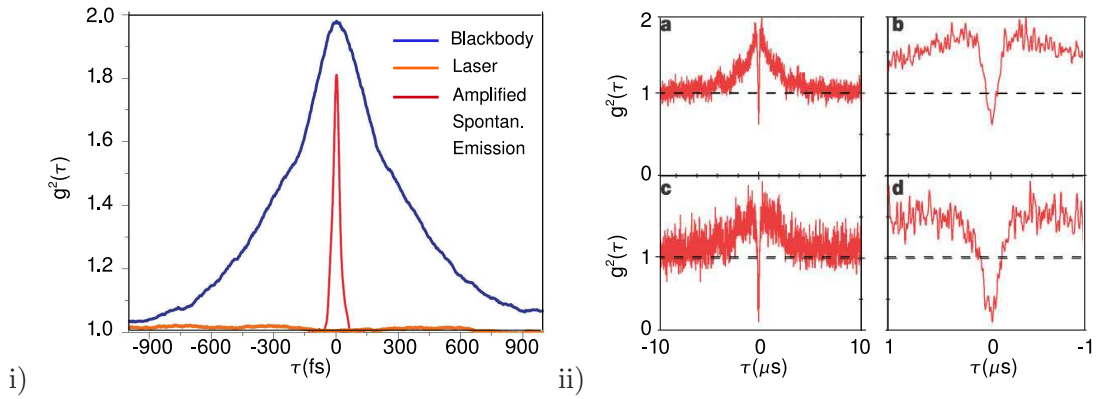

Figure 1.9. i) Recent experimental results of temporal photon bunching for the blackbody radiation showing $g^{(2)}_{class}(\tau) < g^{(2)}_{class}(0)$. The horizontal axes is the delay time τ. Also the condition $g^{(2)}(\tau) = 1$ is obtained in the case of coherent laser beam [Boitier & al.]. ii) Experimental results for the measure of the quantum second-order coherence function, for two different pump intensities a) and c) from one-atom laser in the regime of strong coupling, as an example of temporal photon antibunching [McKeever & al.]. Panels b) and c) are zooms. This picture shows the photon temporal antibunching effect where the correlation at different times, $g^{(2)}(\tau)$, is higher than the correlation between instantaneous photo-detections, $g^{(2)}(0)$. This phenomenon, meaningless for classical fields, can only be described from the quantum theory of light. Complete second-order coherence $g^{(2)}(\tau) = 1$ for every time is also plotted.

the *photon antibunching* effect, i.e. the photons tend to arrive evenly spaced in time (first line in Fig. 1.8), or in space if we are observing spatial antibunching:

$$g^{(2)}(\tau) > g^{(2)}(0). \tag{1.32}$$

Fig. 1.9a shows the experimental realization of a one-atom laser in the regime of strong coupling as an example of temporal photon antibunching [McKeever & al.]. Another example, considered the pioneer work [Kimble & al.], demonstrated how the resonance fluorescence light was antibunched, where the atomic recovery between one emission and the next introduces time delays between successive photons. Other examples are provided by light-emitting devices driven by electron beams or currents, whose mutually repulsive charges acquire characteristic spatial separation that are partly transferred to the emitted photons [Teich & Saleh].

We are interested in the spatial quantum coherence in the far field of an optical beam (obtained by passing the beam through a lens at the appropriate distance). This is equivalent to look at the two point spatial coherence in Fourier space. Spatial antibunching was predicted by [Le Berre & al.(79)] and experimentally proved in [Nogueira & al.]. As our study focus in the spatial transverse profile we will be interesting in the spatial quantum coherence:

$$g^{(2)}(k,-k) = \frac{\langle \hat{a}^\dagger(k)\hat{a}^\dagger(-k)\hat{a}(-k)\hat{a}(k)\rangle}{\langle \hat{a}^\dagger(k)\hat{a}(k)\rangle^2} \tag{1.33}$$

as compared to $g^{(2)}(k,-k) = g^{(2)}(0)$. It is important to sign that the product of the operators is normally ordered (i.e. with the annihilation operators standing to the right of the creation operators, for example, the number operator $\hat{N} = \hat{a}^\dagger a$ is already normally ordered, meaning in common notation, $\hat{N} \equiv: \hat{N} :$). Then, we can rewrite:

$$g^{(2)}(k,-k) = \frac{\langle: \hat{N}(k)\hat{N}(-k) :\rangle}{\langle \hat{N}(k)\rangle^2} \tag{1.34}$$

which is one of the main quantities we will deal in our multimode treatment of the signal field generated by the OPO (see section 4.1), and the spatial antibunching criterion will be:

$$\langle: \hat{N}(k)\hat{N}(-k) :\rangle > \langle \hat{N}(k)\rangle^2. \tag{1.35}$$

Coherent states

Before introducing the squeezed states, we present a set of states, the coherent ones, which give rise to a sensible classical limit, in fact, they set the boundary between classical and quantum states.

We consider for simplicity the case of a single-mode electromagnetic field propagating in the z direction and linearly polarized along the x axes:

$$E_x(z,t) = \sqrt{\frac{2\omega^2}{V\epsilon_0}} q(t)\sin(kz) \tag{1.36}$$

$$B_y(z,t) = \frac{\mu_0\epsilon_0}{k}\sqrt{\frac{2\omega^2}{V\epsilon_0}} \dot{q}(t)\cos(kz) \tag{1.37}$$

where V is the effective volume of the quantization cavity, ϵ_0 the vacuum dielectric constant and $q(t)$ will act as a canonical position, having the dimensions of length. The energy of this single-mode equals:

$$H = \frac{1}{2}\int dV \left(\epsilon_0 E_x^2(z,t) + \frac{1}{\mu_0} B_y^2(z,t)\right) = \frac{1}{2}(p^2 + \omega^2 q^2) \tag{1.38}$$

where as usual, p is the canonical linear momentum of a 'particle' of unit mass. The quantum analogous is the Hamiltonian for the harmonic oscillator. It is obtained by replacing q and p with their corresponding quantum operators, satisfying the canonical conmutation relation:

$$[\hat{q},\hat{p}] = i\hbar\hat{I} \tag{1.39}$$

being $\hat{I}$ the identity operator. In the following, we will take the single-mode case, whose quantum version is obtained substituting q and p in Eq. (1.36) for the analogous quantum operators in the Heisenberg picture. When we write $\hat{q}$ and $\hat{p}$ as functions of the quantum conjugated creation $\hat{a}^\dagger$ and annihilation $\hat{a}$ operators:

$$\hat{q}(t) = \frac{D}{2\omega}(\hat{a}(t) + \hat{a}(t)^\dagger) \tag{1.40}$$

$$\hat{p}(t) = \frac{d}{2i}(\hat{a}(t) - \hat{a}(t)^\dagger) \tag{1.41}$$

where $D = \sqrt{2\hbar\omega}$ and the time dependence of the creation and annihilation operators is given by:

$$\frac{d\hat{a}}{dt} = \frac{i[\hat{H}, \hat{a}]}{\hbar} = -i\omega\hat{a} \tag{1.42}$$

which has the solution $\hat{a}(t) = \hat{a}(0)e^{-i\omega t}$. Then the electric and magnetic fields yields:

$$\hat{E}_x(z,t) = \frac{D}{\sqrt{2\epsilon_0 V}}(\hat{a}(t) + \hat{a}^\dagger(t))\sin(kz) \tag{1.43}$$

$$\hat{B}_y(z,t) = \frac{\mu_0\omega}{ik}\sqrt{\frac{\epsilon_0\hbar\omega^3}{V}}(\hat{a}(t) - \hat{a}^\dagger(t))\cos(kz). \tag{1.44}$$

We can express the Hamiltonian of the electromagnetic field by replacing Eqs. (1.40,1.41) in Eq. (1.38) as:

$$\hat{H} = (\hat{N} + \frac{1}{2})\hbar\omega \tag{1.45}$$

which is the well known Hamiltonian of the quantum harmonic oscillator, in terms of the number operator $\hat{N} = \hat{a}^\dagger\hat{a}$ introduced in the previous section. The eigenstates $\{|n\rangle\}$, such that:

$$\hat{N}|n\rangle = n|n\rangle \tag{1.46}$$

are the number states and they have a well-defined energy as $[\hat{H}, \hat{N}] = 0$. These states do not have a well-defined electric field since:

$$\langle n|\hat{E}_x(z,t)|n\rangle = \frac{D}{\sqrt{2\epsilon_0 V}}\sin(\omega t - kz)(\langle n|\hat{a}|n\rangle + \langle n|\hat{a}^\dagger|n\rangle) = 0 \quad \forall n. \tag{1.47}$$

Still the squared field, related to the energy density, has an expectation value over a number state different from zero:

(1.48)

$$\langle n|\hat{E}_x^2(z,t)|n\rangle = \frac{D^2}{2\epsilon_0 V}\sin^2(\omega t - kz)(\langle n|\hat{a}^{\dagger 2} + \hat{a}^2 + 2\hat{a}^\dagger\hat{a} + 1|n\rangle = \frac{2\hbar\omega}{\epsilon_0 V}\sin^2(\omega t - kz)(n + \frac{1}{2}).$$

Therefore, it is worth to stress that while the mean of the electric field is zero for every energy state, its intensity, proportional to $|E|^2$, is different form zero even for the vacuum

state.

Let us define the variance of a given quantity C', time or ensemble averaged, as:

$$\langle(\Delta C)^2\rangle = \langle C^2\rangle - \langle C\rangle^2 \tag{1.49}$$

and the standard deviation, as usually, $\Delta C = \sqrt{\langle(\Delta\hat{C})^2\rangle}$. It is a general result that the **fluctuations** of the measured quantity:

$$\delta C = C - \langle C\rangle \tag{1.50}$$

are related to the variance by:

$$\langle(\Delta C)^2\rangle = \langle(\delta C)^2\rangle. \tag{1.51}$$

For $n = 0$ we obtain the so-called vacuum fluctuations of the electric field:

$$\langle\Delta^2\hat{E}_x\rangle = \frac{\hbar\omega}{\epsilon_0 V}\sin^2(\omega t - kz) \tag{1.52}$$

It is frequently suggested [Sakurai] that the classical limit of the quantified electromagnetic field is the limit in which the number of photons becomes very large such that the number operator $\hat{N}$ becomes a continuous variable. However, there are macroscopic quantum states where the intensities are continuous variables. Therefore, this cannot be the whole story, since the mean given in Eq. (1.47) is $\langle n|\hat{E}|n\rangle = 0$, no matter how large the value of n. Moreover, at a fixed point in space a classical field oscillates sinusoidally in time, but clearly it does not happen for the expectation value of the field operator for a number state, always null.

The set of states satisfying such correspondence between classical and quantum optics, indeed, are the coherent states $\{|\alpha\rangle\}$. They must be eigenstates of the annihilation operator, i.e.:

$$\hat{a}|\alpha\rangle = \alpha|\alpha\rangle \tag{1.53}$$

in order to not vanish when calculating expectations values of quantities as the electric field are of the form $\langle\alpha|(\hat{a} \pm \hat{a}^\dagger)|\alpha\rangle$. The number states are a complet set so we can expand the coherent states as:

$$|\alpha\rangle = e^{|\alpha|^2/2}\sum_0^\infty \frac{\alpha^n}{\sqrt{n!}}|n\rangle \tag{1.54}$$

Coherent states are the classical limit of quantum states in several senses:

- the expectation value of the electric field has the form of the classical expression:

$$\begin{aligned}\langle\alpha|\hat{E}_x(z,t)|\alpha\rangle &= \frac{D}{\sqrt{2\epsilon_0 V}}(\langle\alpha|\hat{a}|\alpha\rangle + \langle\alpha|\hat{a}^\dagger|\alpha\rangle)\sin(\omega t - kz - \theta) = \\ &= \frac{D}{\sqrt{2\epsilon_0 V}}(\alpha + \alpha^*)\sin(\omega t - kz - \theta) = 2|\alpha|\frac{D}{\sqrt{2\epsilon_0 V}}\sin(\omega t - kz - \theta)\end{aligned} \tag{1.55}$$

where we wrote $\alpha = |\alpha|e^{i\theta}$.

- the fluctuations in the electric field are the same as for the vacuum. It means that coherent states only contain the noise of the vacuum or *shot noise*. In order to obtain the fluctuations we calculate the variance of the $\hat{E}_x(z,t)$ in a coherent state $|\alpha\rangle$, as defined in Eq. (1.49). The expectation value of the squared field reads:

(1.56)
$$\langle\alpha|\hat{E}_x^2(z,t)|\alpha\rangle = \frac{\hbar\omega}{\epsilon_0 V}\sin^2(\omega t - kz)(\langle\alpha|\hat{a}^{\dagger 2} + \hat{a}^2 + 2\hat{a}^\dagger\hat{a} + 1|\alpha\rangle = \frac{\hbar\omega}{\epsilon_0 V}\sin^2(\omega t - kz)((\alpha + \alpha^*)^2 + 1).$$

thus the mean of the squared fluctuations is:

$$\langle(\delta\hat{E}_x)^2\rangle = \langle(\Delta\hat{E}_x)^2\rangle = \frac{\hbar\omega}{\epsilon_0 V}\sin^2(\omega t - kz) \tag{1.57}$$

which coincides with the vacuum fluctuations, Eq. (1.52). They vanish for $\hbar \to 0$ and they do not depend on time, meaning the wave packet of a coherent state bounces back and forth without spreading in shape, as a classical oscillator does.

- the fluctuations in the fractional uncertainty for the photon number decrease with the increasing average photon number:

$$\frac{\Delta\hat{N}}{\langle\alpha|\hat{N}|\alpha\rangle} = \frac{1}{\sqrt{\langle\alpha|\hat{N}|\alpha\rangle}} \tag{1.58}$$

- the probability distribution of photons in a coherent state is a Poissonian distribution [Walls & Milburn]:

$$P(n) = |\langle n|\alpha\rangle|^2 = \frac{|\alpha|^{2n}e^{-|\alpha|^2}}{n!} \tag{1.59}$$

The mean number of photons and the variance coincides:

$$\langle\alpha|\hat{N}|\alpha\rangle \equiv \langle(\Delta\hat{N})^2\rangle = |\alpha|^2 \tag{1.60}$$

which is a characteristic of a Poissonian process. In Fig. 1.10a the probability distribution given in Eq. (1.59) are plotted for three different values of the mean. Then, the states become well localized in phase when increasing average photon number, because for large mean number of photons the Poissonian distribution in Eq. (1.59) may be approximate to a Gaussian becoming narrower when increasing that mean [Gerry].

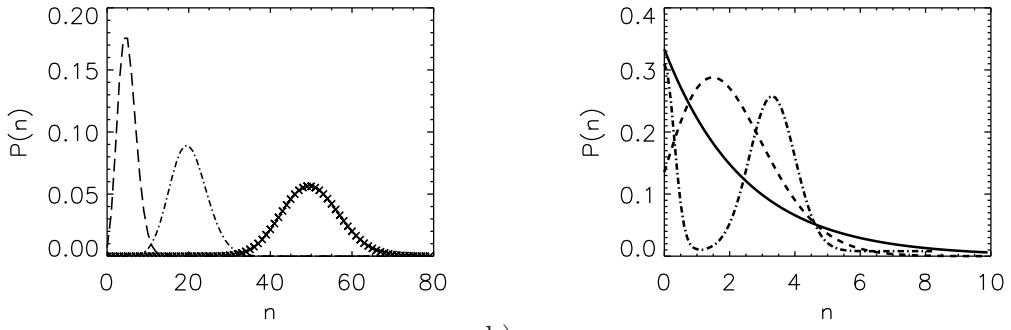

a) b)

Figure 1.10. a) Representation of the Poissonian probability distribution given in Eq. (1.59): $P(n) = |\alpha|^{2n} e^{-|\alpha|^2}/n!$ (valid only for integer numbers) for three different mean values $\langle|\alpha|\hat{N}|\alpha\rangle = |\alpha|^2$. In each case, the mean coincides with the value of the variance $\langle|\alpha\hat{N}|\alpha\rangle \equiv \langle(\Delta\hat{N})^2\rangle$, thus twice, the squared root of the mean gives the 'width' of the bell. b) Pictorial representation (valid only for integer numbers) of Poissonian (dashed line), super-Poissonian (solid line) and sub-Poissonian distributions (dot-dashed line). As we said, for states exhibiting Poissonian distribution the number operator variance equals the mean, as in coherent states, and its fluctuations take the minimum values, i.e. equals to those in vacuum. In the super-Poissonian case, the variance exceeds the mean. By contrast, in the sub-Poissonian statistic, the variance is smaller than the mean, therefore they fulfill the condition to be quantum states, as may occur to antibunched states (studied in the previous section) and to squeezed states, described in the next section.

Sub-Poissonian states and Spatial Antibunching

Physically, Poisson distribution describes the number of photoncounts in a series of experiments that observe a light beam with the same mean intensity (meaning the average of the intensity over a cycle of the oscillation at a given frequency, termed $\langle I\rangle_{cycle}$) in the case of time independent $\langle I\rangle_{cycle}$ or when the integration time is much longer that the characteristic time scale of the intensity fluctuations, τ_c.

For thermal or chaotic states the fluctuations of $\hat{N}$ are larger than in coherent light (shot noise). An example is shown in dashed line in Fig. 1.10b. Light whose photon-number variance exceeds $\langle\alpha|\hat{N}|\alpha\rangle$, as in thermal or chaotic light, is said to exhibit super-Poissonian fluctuations, as the solid line in Fig. 1.10b shows. Remembering the former section, it is easy to show [Gerry] that quantum coherent states are second-order coherent. Light whose photon-number variance falls below the value $\langle\alpha\hat{N}|\alpha\rangle$ is sub-Poissonian.

If normal ordered variance are considered, the sub-Poissonian condition:

$$\langle(\Delta\hat{N})^2\rangle < \langle\hat{N}\rangle \tag{1.61}$$

becomes:

$$\langle{:}\,(\Delta\hat{N})\,{:}\rangle < 0 \tag{1.62}$$

that is a negative variance. This feature defines a new class of light state with non classical behavior, called sub-Poissonian.

Squeezed states

We now introduce quadrature operators regarding the canonical position and momentum introduced before in Eqs. (1.40,1.41):

$$\begin{aligned} \hat{X}_1 &= (\hat{a} + \hat{a}^\dagger) \\ \hat{X}_2 &= \tfrac{1}{i}(\hat{a} - \hat{a}^\dagger). \end{aligned} \tag{1.63}$$

The electric field operator becomes

$$\hat{E}_x(z,t) = 2\frac{D}{\sqrt{\epsilon_0 V}} \sin(kz)(\hat{X}_1 \cos(\omega t) + \hat{X}_2 \sin(\omega t)). \tag{1.64}$$

For our further purposes it is convenient to introduce generic quadrature operator:

$$\hat{X}(\vartheta) = \hat{a}e^{i\vartheta} + \hat{a}^\dagger e^{-i\vartheta} \tag{1.65}$$

where we recover $\hat{X}_1$ for $\vartheta = 0$ and $\hat{X}_2$ for $\vartheta = -\pi/2$. We can understand the operators $\hat{X}_1$ and $\hat{X}_2$ as amplitude oscillating with a relative phase equals $\pi/2$, so, in quadrature. They fulfill the same commutation relation than the canonical position and momentum but scaled to be dimensionless: $[\hat{X}_1, \hat{X}_2] = 2i$. Appling the Heisenberg Uncertainty Principle for the quadrature operators we draw:

$$\Delta\hat{X}_1 \Delta\hat{X}_2 = \sqrt{\langle(\Delta\hat{X}_1)^2\rangle}\sqrt{\langle(\Delta\hat{X}_2)^2\rangle} \geq \frac{1}{2}|\langle[\hat{X}_1, \hat{X}_2]\rangle| = 1 \tag{1.66}$$

(for a derivation, see [Gardiner]). Knowing the variances of the quadrature operators for coherent states:

$$\langle(\Delta\hat{X}_1)^2\rangle = \langle(\Delta\hat{X}_2)^2\rangle = 1 \tag{1.67}$$

we see that the uncertainties in both quadratures over the coherent states minimize the uncertainty product:

$$\Delta\hat{X}_1 \Delta\hat{X}_2 = 1. \tag{1.68}$$

Even if well known quadrature operators, $\hat{X}_1$ and $\hat{X}_2$, are related to the canonical position an momentum, it is that quantum states cannot be represented by a point in phase space, as it is in classical mechanics. Nevertheless, it is possible to introduce some quasi-probability' on the complex α-plane, as we will discussed later. Such plane plays the role of phase space where, up to scale factors, the real an imaginary parts of α are the

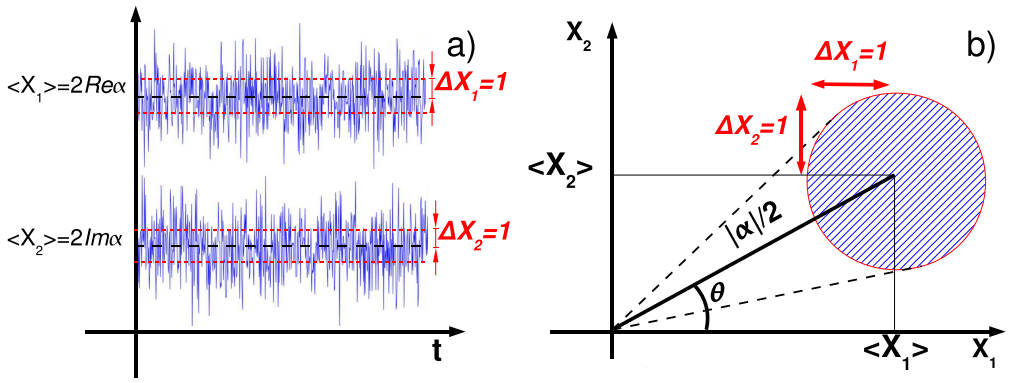

Figure 1.11. Quantum coherent state of amplitude $|\alpha|$ and phase angle θ where $Re\alpha > Im\alpha$. a) Time evolution of the fluctuations of both quadratures around the corresponding mean value $\langle\alpha|\hat{X}_1|\alpha\rangle = 2Re\alpha$ and $\langle\alpha|\hat{X}_1|\alpha\rangle = 2Re\alpha$. b) Remembering Eq. 1.67: $\langle(\Delta\hat{X}_1)^2\rangle = \langle(\hat{X}_2)^2\rangle = 1$ for all $|\alpha\rangle$, it is clear that the error circle is the same for all coherent states with radio equal 1. Phase space portrait of the quantum vacuum state , as $|\alpha| = 0$, has the circle centered in the coordinates origin.

position and momentum variables respectively since $2Re\alpha \equiv \langle\alpha|\hat{X}_1|\alpha\rangle = (\alpha + \alpha^*)$ and $2Im\alpha \equiv \langle\alpha|\hat{X}_2|\alpha\rangle = (\alpha - \alpha^*)/i$. Then, a coherent state $|\alpha\rangle$ with $\alpha = |\alpha|e^{i\theta}$ may be represented as in the right panel of Fig. 1.11 where the shaded area represents the area of uncertainty resulting from the fluctuations in all directions of phase space. As they are equal, this area is a circle. Moreover, they are independent of α and identical to those in the vacuum. For the vacuum state $|\alpha| = 0$, the circle is centered in the coordinates origin.

Now we introduce one of the most important example of non classical states, called squeezed states. As for a coherent state $|\alpha\rangle$ the variances of two quadratures fulfill: $\langle(\Delta\hat{X}_1)^2\rangle = \langle(\Delta\hat{X}_2)^2\rangle = 1$, coherent states minimize the Heisenberg Uncertainty Principle, (as we already said they only contains the fluctuations of the vacuum). States for which:

$$\langle(\Delta\hat{X}_1)^2\rangle < 1 \quad or \quad \langle(\Delta\hat{X}_2)^2\rangle < 1 \tag{1.69}$$

are known as squeezed states. They will have less noise in one or the quadratures than for a coherent state, i.e. the fluctuations in that quadrature are squeezed (see Fig. 1.12) and we say that the fluctuations are below the shot noise level [Stoler], that is the level of fluctuations of a coherent state . Of course, the fluctuations in the other quadrature must be enhanced so as to not violate the uncertainty relation. There are squeezed states for which the inequality given Eq. (1.66) becomes an equality, but in general they do not need to be minimum uncertainty states.

When deriving the dynamics of the electromagnetic field it is not always possible to write mode excitations as a linear superposition of basic coherent $|\alpha\rangle$ or number $|n\rangle$ states, that is a pure state. When we deal with a general electromagnetic field we should describe an

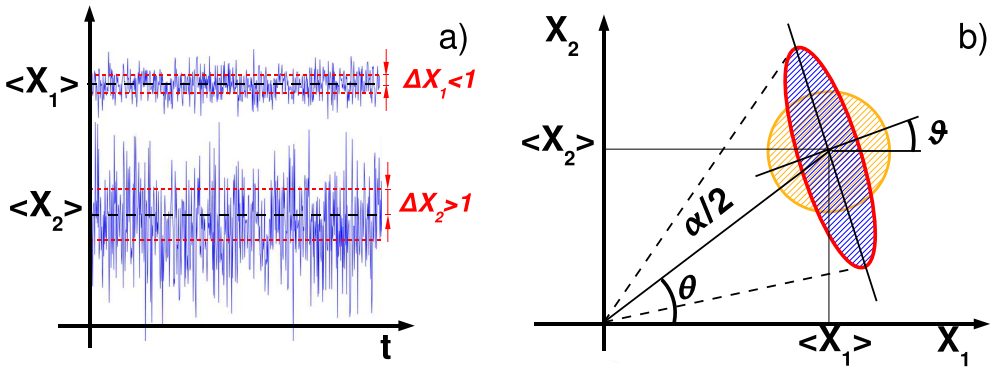

Figure 1.12. Quadrature squeezed state. a) Time evolution of the fluctuations of both quadratures around the corresponding mean value for $Re\alpha > Im\alpha$. As the fluctuations in the $\hat{X}_1$ quadrature are reduced with respect to the coherent state case showed in Fig 1.11, this is an amplitude squeezed state. b) Amplitude squeezed state represented in the phase-space of α-complex plane, where the fluctuations in phase θ , i.e. the angle substenting the arc limited by the dashed lines, become larger than for a coherent state, in yellow. This kind of states, also known as photon-number squeezed states, exhibit sub-Poissonian probability distribution because their photon number fluctuations, related to $\langle \hat{N} \rangle = |\alpha|^2$ are below the shot noise level. For values of the rotational angle such as $\pi/2 < \vartheta < 3\pi/2$, we have a phase squeezed state, where now the number of photons is more delocalized while the noise in the phase θ is reduced. These states are super-Poissonian distributed. The error ellipse for a squeezed vacuum state would be center in the origin of coordinates.

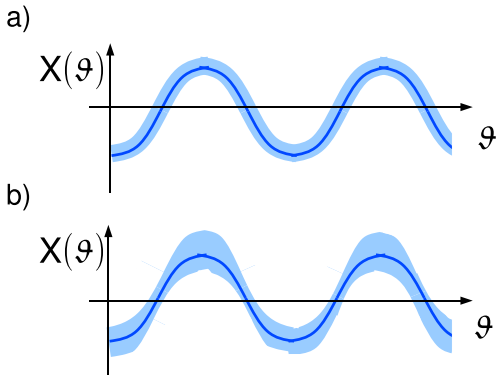

Figure 1.13. Pictorial representation the generic quadrature $\hat{X}(\vartheta) = \hat{a}e^{i\vartheta} + \hat{a}^\dagger e^{-i\vartheta}$ where $\hat{X}_1$ corresponds to $\vartheta = 0$ and $\hat{X}_2$ to $\vartheta = \pi/2$. In dark blue is the average quadrature and the noise or variance is represented in soft blue. In the picture (a) the quadrature is represented for a coherent state. As the variance of both quadratures (for all coherent states) are $\langle (\Delta\hat{X}_1)^2 \rangle = \langle (\Delta\hat{X}_2)^2 \rangle = 1$, the fluctuation region has a constant width. The picture (b) is a squeezed state, where the fluctuations decrease and increase within the interval given for Eq. (1.84), $-1 \leq \langle : (\Delta\hat{X}(\vartheta))^2 : \rangle < 0$, as the ellipse rotates in the α-plane by varying ϑ (see Fig. 1.12).

infinite number of modes, each one with (in principle) infinite number of possible quantum states.

Our photons are thermally excited in the modes of a cavity. They are an example of statistical mixture, because we only can achieve to calculate the probability of the field to be found in a state, which is itself a linear combination of basic number states $|n\rangle$. We will show how statistical distributions are introduced into quantum mechanics by means of the density operator. A given electromagnetic field is in a cavity in the state $|u\rangle$ with probability P_u and 'u' labels enough states in order to completely describe the system (for example, it runs over a finite set of coherent states $\{|\alpha\rangle\}$). If u' labels number states, P_n is a probability distribution giving the probability of having n photons in the mode. Taking the observable O that is represented by a quantum-mechanical operator $\hat{O}$ the expected value of the observable for the state $|u\rangle$ is $\langle u|\hat{O}|u\rangle$ and hence the ensemble average of the observable for the statistical mixture specified by P_u is:

$$\langle\hat{O}\rangle = \Sigma_u P_u \langle u|\hat{O}|u\rangle \tag{1.70}$$

It will be assumed that P_u is a normalized probability distribution

$$\Sigma_u P_u = 1 \tag{1.71}$$

The same expression can be written involving the density operator as follows. Let $|S\rangle$ represent some complete set of states for the fields considered S being a label that can take a series of values. Then according to the closure theorem:

$$\Sigma_S |S\rangle\langle S| = 1 \tag{1.72}$$

Insertion of this unit quantity immediately after the operator $\hat{O}$ in Eq. 1.70 gives:

$$\langle\hat{O}\rangle = \Sigma_u \Sigma_S P_u \langle S|u\rangle\langle u|\hat{O}|S\rangle \tag{1.73}$$

The density operator $\hat{\rho}$ is defined to be:

$$\hat{\rho} = \Sigma_u P_u |u\rangle\langle u| \tag{1.74}$$

then the average value of O can be written:

$$\langle\hat{O}\rangle = \Sigma_S \langle S|\hat{\rho}\hat{O}|S\rangle \tag{1.75}$$

The density operator contains exactly the same information as the probability distribution P_u and $\hat{\rho}$ is determined once the P_u are specified for a given set of pure states $|u\rangle$ and it can be shown that the general result of $\langle\hat{O}\rangle$ is independent of the particular complete set

of states $|S\rangle$ chosen for the evaluation, so we can chose those in which it is diagonal and the trace is invariant under change of basis. Then the last equation can be written

$$\langle \hat{O} \rangle = Tr(\hat{\rho}\hat{O}). \tag{1.76}$$

The density operator has $Tr\hat{\rho} = \sum_i p_i = 1$ and it allows as to calculate the expectation value of an operator over mixed states.
The closure relation for the coherent states is given as an integral over the complex α-plane according to:

$$\int |\alpha\rangle\langle\alpha| \frac{d^2\alpha}{\pi} = 1 \tag{1.77}$$

where $d^2\alpha = dRe(\alpha)dIm(\alpha)$. Then we can express the density operator in terms of the coherent states as:

$$\hat{\rho} = \int P(\alpha)|\alpha\rangle\langle\alpha| d^2\alpha \tag{1.78}$$

where $P(\alpha)$ is a weight function known as the **Glauber-Sudarshan P distribution** and is analogous to the phase-space representations of statistical mechanics. It is then generally called quasiprobability distribution. As we would expect: $Tr\hat{\rho} = \int P(\alpha) d^2\alpha = 1$ and the P function is real since $\hat{\rho}$ is Hermitian. But the coherent states are not orthogonal:

$$| < \beta|\alpha > |^2 = e^{-|\alpha-\beta|^2} \tag{1.79}$$

equal unity only in the limit $\alpha - \beta >> 1$, so the set is overcomplete. Then, the representation has rather exotic properties [Walls & Milburn]. For instance, it can be shown by applying the definition of P to a pure coherent sate $|\beta\rangle$ where $\hat{\rho} = |\beta\rangle\langle\beta|$ that $P(\alpha)_{|\beta\rangle} = \delta^2(\alpha - \beta)$. Moreover, in the case of a pure number state $|n\rangle$ with $\hat{\rho} = |n\rangle\langle n|$ it is found:

$$P(\alpha)_{|n\rangle} \propto \frac{\partial^{(2n)}}{\partial\alpha^n \partial\alpha^{*n}} \delta^2(\alpha). \tag{1.80}$$

Therefore, there are quantum states for which $P(\alpha)$ is highly singular (more singular than a delta) and can even be negative. These states are called 'non classical'. States in the α-plane for which $P(\alpha)$ is positive or not more singular than a delta function are, in this sense, classical. Coherent states, which are close to what we would expect for classical oscillating fields as disused above, have P distributions given by delta functions. Thus they are classical in the sense described here. Certain effects, as antibunching and squeezing we have already described, can occur only for states for which the P distribution is negative or highly singular.
It is worth to stress that a quasi-probability as here defined can be used as a not approximated alternative to the density operator to describe the dynamics of an optical system,

thanks to the Optical Equivalence Theorem we will describe in the next section. Let us consider quadrature squeezing. We calculate:

$$\langle(\Delta\hat{X}_1)^2\rangle = \frac{1}{4}\{1 + \int P(\alpha)[(\alpha+\alpha^*) - (\langle\hat{a}\rangle + \langle\hat{a}^\dagger\rangle)]^2 d^2\alpha\} \tag{1.81}$$

and

$$\langle(\Delta\hat{X}_2)^2\rangle = \frac{1}{4}\{1 + \int P(\alpha)[(\alpha-\alpha^*)/i - (\langle\hat{a}\rangle - \langle\hat{a}^\dagger\rangle)/i]^2 d^2\alpha\}. \tag{1.82}$$

Because the term inside the square bracket is always positive, the squeezing condition (Eq. 1.69) requires that $P(\alpha)$ be nonpositive at least in some regions of phase space. Remembering the definition of the generic quadrature operator (Eq. 1.65):

$$\hat{X}(\vartheta) = \hat{a}e^{-i\vartheta} + \hat{a}^\dagger e^{i\vartheta} \tag{1.83}$$

we can introduce the normally ordered variance (where the creation operators stand on the left), $\langle: (\Delta\hat{X}(\vartheta))^2 :\rangle$ such that squeezing exists whenever:

$$-1 \leq \langle: (\Delta\hat{X}(\vartheta))^2 :\rangle < 0. \tag{1.84}$$

The effects of the losses of the cavity have been extensively studied also in relation to squeezed states and twin beams phenomena. Generally, the cavity losses decrease the quantum effects present inside the cavity [Graham]. The important point is how to link the intracavity results with the observable external cavity elds. In [Collett & Gardiner] there is developed an input/output formalism for optical cavities in order to obtain the behavior of the fields outside the cavity, given the fields inside the cavity. It is shown that correlations in normal ordering calculated inside the cavity are reduced with respect to their value outside in a factor 2. Then, the quadrature squeezing occurs for normal ordering variances in the interval:

$$-0.5 \leq \langle: (\Delta\hat{X}(\vartheta))^2 :\rangle < 0. \tag{1.85}$$

About how to build squeezed states, the most common scheme involves the Optical Parametric Oscillator (introduced in section 1.2.1), which produces squeezed states of light through the non linear process of down conversion in which photon pairs are created. The simplest squeezing operator (squeezed states may be also produced by four-wave-mixing processes) is:

$$\hat{S}(\xi) = e^{\frac{1}{2}(\xi^*\hat{a} - \xi\hat{a}^{\dagger 2})} \tag{1.86}$$

and it generates a squeezed state when acting on a coherent or vacuum state, with squeezing parameter ξ. The relation with squeezing is evident by recovering the Parametric Down Conversion Hamiltonian Eq. (1.5):

$$\hat{H}_I = i\hbar\chi^{(2)}(\beta^*\hat{a}^2 - \beta\hat{a}^{\dagger 2})$$

The temporal evolution operator $U = e^{\frac{i}{\hbar}\hat{H}t}$ for the Parametric Down Conversion shows exactly the quadratic dependence leading to squeezing for squeezing parameter $\xi = 2\chi^{(2)\beta t}$. Let us now focus on the measurement of squeezed states. Because there are certain values of the phase where the electric field uncertainty becomes small, a phase-sensitive form of detection (homodyning) is used for the detection of quadrature-squeezed light [Teich & Saleh]. Homodyne detection is used to extract the quadrature of the eld with reduced fluctuations. In the single-ended conguration, the squeezed light is combined at an unequal beam-splitter with coherent light from a laser local oscillator (LO). If the LO phase is chosen properly the superposition eld will be photon-number squeezed, resulting in a sub-shot-noise spectrum. The first observation of squeezing was achieved in 1985 by [Slusher & al.] in an experiment of parametric generation involving four-wave mixing in sodium vapor (Kerr media). Recent experiments have achieved even 90% squeezed light [Vahlbruch & al.]. As we have already pointed, due to the reduced level of noise in proper observables (quadratures) of squeezed states, their use has been proposed for technological applications [Giovannetti & al]. It has been proposed many years ago and this is now implemented for gravitational waves detection with large scale interferometers [Goda], which deal with such a weak signal that are in the range of quantum fluctuations.

1.4 Phase space description in Quantum Optics and Optical Equivalence Theorem

Equations of motion for the expectation values of system operators may directly be derived from the operator Master equation discussed in the next chapter. Using the quasi-probability representations for the density operator the Master equation for operators may be converted to a differential equation for the distribution. In some cases this will be a Fokker-Planck equation that using methods familiar in stochastic processes may be converted into an equivalent set of stochastic differential equations. Hereby we introduce such quasi-probability distributions and we leave the derivation of the equations for Chapter 2.

Quasi-probability distributions

The P quasi-probability distribution function was introduced in section 1.3. We can, under suitable conditions, represent other operators beside $\hat{\rho}$ in the 'diagonal' coherent state form sometimes called the P-representation, For operator $\hat{B}$, the P-representation is:

$$\hat{B} = \int B(\alpha, \alpha^*)_P |\alpha\rangle\langle\alpha| d^2\alpha. \tag{1.87}$$

The average of $\hat{B}$ is given by (Eq. 1.76):

$$\begin{aligned}\langle\hat{B}\rangle = Tr(\hat{\rho}\hat{B}) = \textstyle\sum_n \langle n|\Big(\int \hat{\rho}B_P(\alpha,\alpha^*)|\alpha\rangle\langle\alpha|d^2\alpha\Big)|n\rangle = \\ = \int B_P(\alpha,\alpha^*)\langle\alpha|\hat{\rho}|\alpha\rangle d^2\alpha.\end{aligned} \tag{1.88}$$

Then the expectation value of the density operator with respect to the coherent state also plays the role of a phase- provability distribution, This is usually called the Q, or Husimi, function:

$$Q(\alpha) = \langle\alpha|\hat{\rho}|\alpha\rangle/\pi. \tag{1.89}$$

According to the properties of the density operator and the product of coherent states (Eq 1.79) Q is clearly a non-negative and bounded distribution: $0 \leq Q(\alpha) > 1/\pi$. The most important property of this representation is that it satisfies the requirements for a true probability distribution. The evolution of a physical state, corresponding to an hermitian density operator, in the Q representation will always be positive and well-behaved [Gardiner] unlike the P representation that may be negative and highly singular, meaningless from a classical point of view.

Characteristic Functions

Let us consider a classical random variable x distributed according to $\rho(x)$, a classical distribution: $\rho(x) \geq 0$ and $\int \rho(x)dx = 1$ with moments defined as:

$$\langle x\rangle = \int dx x^n \rho(x). \tag{1.90}$$

If all moments are known $\hat{\rho}$ is completely defined as can be see by introducing the characteristic function:

$$C(k) = \langle e^{ikx}\rangle = \int dx e^{ikx}\rho(x) = \sum_n^\infty \frac{(ik)^n}{n!}\langle x^n\rangle. \tag{1.91}$$

The probability density is just the Fourier transform of the characteristic function:

$$\rho = \frac{1}{2}\int dk e^{-ikx}C(k). \tag{1.92}$$

And the other way around, once we know the characteristic function, we can calculate the moments:

$$\langle x^n\rangle = \frac{1}{i^n}\frac{d^nC(k)}{dk^n}|_k = 0. \tag{1.93}$$

Now we introduce the two quantum mechanical characteristic functions we are interested in:

$$\begin{aligned}C_N(\lambda) = Tr(\hat{\rho}e^{\lambda\hat{a}^\dagger}e^{-\lambda^*\hat{a}}) \quad Normally\ \ ordered \\ C_A(\lambda) = Tr(\hat{\rho}e^{-\lambda\hat{a}^\dagger}e^{\lambda^*\hat{a}}) \quad Antinormally\ \ ordered\end{aligned} \tag{1.94}$$

also described in terms of the s-parametrized function ([Cahill & Glauber]):

$$C(\lambda, s) = Tr(\hat{\rho} e^{\lambda \hat{a}^\dagger - \lambda^* \hat{a} + s|\lambda|^2/2}) \tag{1.95}$$

where $s = +1$ corresponds to normally ordered characteristic function and $s = -1$ to the antinormal.

We remind that normal ordering, noted as ::, has annihilation operators standing to the right of the creation operators, while it is the opposite for antinormal ordering, noted as $:\!:\!:$.

Then, by extending the moments calculations to correlations:

$$\begin{aligned} \langle (\hat{a}^\dagger)^m \hat{a}^n \rangle &= Tr(\hat{\rho}(\hat{a}^\dagger)^m \hat{a}^n) = \frac{\partial^{(m+n)}}{\partial \lambda^m \partial (-\lambda^*)^n} C_N(\lambda)|_\lambda = 0 \\ \langle (\hat{a})^m (\hat{a}^\dagger)^n \rangle &= Tr(\hat{\rho}(\hat{a})^m (\hat{a}^\dagger)^n) = \frac{\partial^{(m+n)}}{\partial \lambda^n \partial (-\lambda^*)^m} C_A(\lambda)|_\lambda = 0. \end{aligned} \tag{1.96}$$

the antinormally ordered characteristic function may be written as:

$$C_A(\lambda) = Tr(\hat{\rho} e^{-\lambda \hat{a}^\dagger} e^{\lambda^* \hat{a}}) = \frac{1}{\pi} \int d^2\alpha \langle \alpha | e^{\lambda \hat{a}^\dagger} \hat{\rho} e^{-\lambda^* \hat{a}} | \alpha \rangle = \int d^2\alpha Q(\alpha) e^{\lambda \alpha^* - \lambda^* \alpha} \tag{1.97}$$

which is just a two-dimensional Fourier transform of the Q function, so the inversion transform yields:

$$Q(\alpha) = \frac{1}{\pi^2} \int d^2\lambda C_A(\lambda)(\alpha) e^{\lambda^* \alpha - \lambda \alpha^*}. \tag{1.98}$$

Writing $\hat{\rho}$ in the P-representation in the normally ordered characteristic function we obtain:

$$C_N(\lambda) = Tr(\hat{\rho} e^{\lambda \hat{a}^\dagger} e^{-\lambda^* \hat{a}}) = \int d^2\alpha P(\alpha) \langle \alpha | e^{\lambda \hat{a}^\dagger} e^{-\lambda^* \hat{a}} | \alpha \rangle = \int d^2\alpha P(\alpha) e^{\lambda \alpha^* - \lambda^* \alpha} \tag{1.99}$$

giving:

$$P(\alpha) = \frac{1}{\pi^2} \int d^2\lambda C_N(\lambda)(\alpha) e^{\lambda^* \alpha - \lambda \alpha^*}. \tag{1.100}$$

From operators to functions in the phase-space

As we said in the beginning of this section, a standard method to describe the dynamics of a quantum system is through differential equations for stochastic fields (suitable for numerical computing) rather than using the Master equation for the density operator. Essentially, it means that instead of performing calculations in quantum operator formalism, it is possible to map such operators into the quasi-probabilities distributions. That is basis of the Optical Equivalence Theorem [Sudarshan] that reads:

Theorem 1.4.1. *The expectation value of a normally ordered operator is just the P quasi-probability function weighted average of the function obtained from the operator by the replacements $\hat{a} \to \alpha$ and $\hat{a}^\dagger \to \alpha^*$.*

Equivalent statement can be done for the Q representation (used in the following chapters) with antinormally ordered operators. Then, a representation or quasi-probability function is a tool which allows us to pass from the dynamics of operators to the dynamics of functions α_i, α_i^* in the phase space.Summarizing:

$$< \hat{a}^\dagger \hat{a} > \quad \longleftrightarrow \quad < \alpha^* \alpha >_P \tag{1.101}$$

$$< \hat{a} \hat{a}^\dagger > \quad \longleftrightarrow \quad < \alpha^* \alpha >_Q \tag{1.102}$$

In the next chapter, when we discuss the mathematical model of our prototype system, we will apply this formalism.

2

The PCOPO model

2.1 OPO with Photonic Crystal (PCOPO)

Our prototype system is an Optical Parametric Oscillator (OPO) with an intracavity Photonic Crystal (photonic crystal), in the following PCOPO, and it is represented in Fig. 2.1. We are interested in a photonic crystal periodically modulated in the transverse profile, thus preventing certain transverse wavelengths to exist. In the previous chapter we have reviewed some the non linear and quantum phenomena taking place in OPO. The model introduced here will be used to study the action of photonic crystal on such phenomena by controlling spatial instabilities threshold as well as quantum phenomena.

In this Master thesis we focus not only on the classical dynamics of the electromagnetic field in PCOPO but also the quantum correlations between spatial modes. Therefore, we consider a full **multimode** Hamiltonian. Moreover, previous works have been done in singly-resonant cavities (where only the signal field was considered) while hereby we consider the doubly-resonant cavity, leading to a **cubic** Hamiltonian in the field operators. Even if the results presented in this work are mostly related to a regime (below threshold) that would be also appropriately described by an approximated quadratic Hamiltonian, we stress that the model here introduced is valid to describe also full non linear dynamics of the PCOPO and this is in fact our ongoing research activity.

As we deal with a general electromagnetic field we should describe an infinite number of modes, each one with (in principle) infinite number of possible quantum states. To describe the intracavity dynamics in a Degenerate OPO we introduce the boson spatial modes $\hat{A}_0(x,t)$ and $\hat{A}_1(x,t)$, respectively at the pump frequency 2ω, and signal frequency ω, where x denotes the transverse coordinate while the z direction dependence is averaged out within a mean field approximation. Standard equal-time commutation relations for

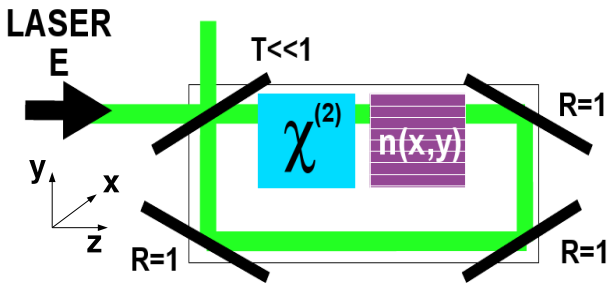

Figure 2.1. Optical Parametric Oscillator with Photonic Crystal (PCOPO) modulated in the transverse profile scheme. We call z the longitudinal coordinate and x, y the transverse coordinates. As reported in the introduction, we consider a cavity formed by four mirrors, two orthogonal to the axis z with a distance L and transmission coefficient $T << 1$, and two orthogonal to the axis x with the distance b and 100% reflectivity. The cavity is filled with a non linear medium ($\chi^{(2)}$) and as novelty, an intracavity photonic crystal with refractive index $n = n(x)$ is embedded. A coherent, stationary, plane-wave laser beam E is longitudinally injected into the cavity, and it is strong enough to be considered undepleted when the energy is transferred from the pump beam to the signal and idler fields in the Degenerated Parametric Down Conversion $2\omega \rightarrow \omega + \omega$. We assume that the input and the internal cavity fields are linearly polarized.

the intracavity fields are then:

$$\left[\hat{A}_i(x,t), \hat{A}_j^{\dagger}(x',t)\right] = \delta_{ij}\delta(x-x')\,, \quad i,j = 0,1. \tag{2.1}$$

Now let us consider the total system (cavity + environment): generally we have only statistical information about the state of the environment, so that, instead of the total wave-function, the total density operator $\hat{\rho}_{tot}$ is introduced [Huang]. In the Schrödinger picture the evolution of $\hat{\rho}_{tot}$ is described by the von Neumann equation:

$$\frac{\partial \hat{\rho}_{tot}}{\partial t} = \frac{1}{i\hbar}[\hat{H}_{tot}, \hat{\rho}_{tot}] \tag{2.2}$$

where $\hat{H}_{tot}$ is the Hamiltonian describing the cavity, the environment and their interactions. We are interested in the properties of the system alone, so we need only the evolution equation for the reduced density operator $\hat{\rho}$ of the intracavity fields, obtained by taking the trace over the degrees of freedom of the environment:

$$\hat{\rho}(t) = Tr_{env}(\hat{\rho}_{tot}). \tag{2.3}$$

For a detailed derivation of the dynamical- equation for the reduced density matrix in presence of dissipation see, for instance, [Carmichael]. The intracavity dynamics is described by a Master equation for the reduced density operator $\hat{\rho}$:

$$\frac{\partial \hat{\rho}}{\partial t} = \frac{1}{i\hbar}[\hat{H}, \hat{\rho}] + \hat{\Lambda}\hat{\rho} \tag{2.4}$$

being $\hat{H}$ the Hamiltonian of the intracavity fields. The Liouvillian $\hat{\Lambda}$ is a super-operator accounting for dissipation (with strength γ) through the partially reecting cavity mirror:

$$\hat{\Lambda}\hat{\rho} = \sum_{i=0,1} \gamma_i \int d^2x \left\{ [\hat{A}_i(x), \hat{\rho}\hat{A}_i^\dagger(x)] + [\hat{A}_i(x)\hat{\rho}, \hat{A}_i^\dagger(x)] \right\}. \tag{2.5}$$

The Master equation has two terms: a strong coupling term describing the intracavity modes couplings, having the same form as in the absence of dissipation, and the dissipative term having the same form it would have in the absence of the strong Hamiltonian coupling. The most important assumption done to obtain Eq. (2.4) is the Markov approximation. In this approximation we assume that there are two different time scales in the total system respectively given by the decay time of the (intracavity) system and of the environment. When the environment and the system evolve in the same time scales, the Markovian approximation is not valid and we cannot obtain a Master equation. When there is a fast evolution of the environment, we can neglect the time needed for the equilibration of the environment and we then obtain Eqs. (2.5, 2.4).
The Hamiltonian operator for our system is a function of fields operators $\hat{A}_0(x,t)$ and $\hat{A}_1(x,t)$, as given, for instance, in [Zambrini & al. (03)]:

$$\hat{H} = \hat{H}_0 + \hat{H}_{int} + \hat{H}_{ext}. \tag{2.6}$$

For our purposes it is important to explicitly consider the spatial dependence. The first part of the Hamiltonian is:

$$\hat{H}_0 = i\hbar \int dx \sum_{i=0,1} \left[\gamma_i \hat{A}_i^\dagger(\vec{x})(\Delta_i - a_i\nabla^2)\hat{A}_i(x) \right] \tag{2.7}$$

and describes the free propagation of the fields inside the cavity, where γ_i are the cavity decay rates, Δ_i the cavity detunings, a_i the diffraction constants. Then:

$$\hat{H}_{ext} = i\hbar \int dx E \left[\hat{A}_0^\dagger(x) - \hat{A}_0(x) \right] \tag{2.8}$$

is due to the interaction with the external pump E at frequency 2ω, which we choose to be real, and

$$\hat{H}_{int} = i\hbar \frac{g}{2} \int dx \left[\hat{A}_0(x)\hat{A}_1^{\dagger 2}(x) - \hat{A}_0^\dagger(x)\hat{A}_1^2(x) \right] \tag{2.9}$$

with g the non linear coefficient, is the interaction term between first and second harmonic due to the non linearity of the system, which is the multimode version of the one introduced in the Chapter 1 when describing the Degenerate Parametric Down Conversion process Eq. (1.5).
It is worth to remark that with respect to introductory OPO treatments in Quantum

Optics books [Loudon], [Walls & Milburn] here we deal with a full multimode model, even in the simplest case of homogeneous classical pump field, i.e. $\hat{A}_0(x) \to A_0$, under Fourier transformation we find:

$$\hat{\hat{H}}_{int} = = i\hbar\frac{g}{2}\int dx\Big[A_0\int dk\hat{\hat{A}}_1^\dagger(k)e^{-ikx}\int dk'\hat{\hat{A}}_1^\dagger(k')e^{-ik'x} - A_0^*\int dk\hat{\hat{A}}_1(k)e^{ikx}\int dk'\hat{\hat{A}}_1(k')e^{ik'x}\Big] =$$
$$= i\hbar\frac{g}{2}\int dk\left[A_0\hat{\hat{A}}_1^\dagger(k)\hat{\hat{A}}_1^\dagger(-k) - A_0^*\hat{\hat{A}}_1(k)\hat{\hat{A}}_1(-k)\right]$$

in which we recognize a sum of terms $(\hat{a}_k^\dagger\hat{a}_{-k}^\dagger + h.c)$ as in a Non Degenerated Parametric Down Conversion.

2.2 From the Master equation to Langevin equations

Some problems are studied expanding the density operator $\hat{\rho}$ in the Fock space

$$\hat{\rho} = \sum_{n,m} c_{nm}|n\rangle\langle m| \tag{2.11}$$

but there are important disvantages. The coefficients $c_{n,m}$ are c-numbers and there is an infinite number of them. It could be possible to truncate the infinite sum at some given order but many times we need phase-dependence properties of the electromagnetic field and the full expansion is required. More suitable for our work are expansions in terms of the quasi-probability distributions introduced in section 1.4. In the following, we will describe the procedure to obtain the Langevin equations, which are stochastic differential equations that can be simulated numerically, when starting from the Master equation for $\hat{\rho}$. A scheme with a summary of the procedure we will describe in this section is shown in Fig. 2.2.

An operator Master equation, Eq. (2.4), is transformed into a complex equation for a quasi-probability representation for the density operator. For the sake of clarity, here we are considering a generic Hamiltonian for one field operator $\hat{a}$, such as:

$$\hat{H} = f(\hat{a}, \hat{a}^\dagger). \tag{2.12}$$

It is necessary to first establish the rules for converting products of operators $\hat{a}$ and $\hat{a}^\dagger$ with the density $\hat{\rho}$ into an equivalent functional form [Zambrini]:

$$\begin{aligned}
\hat{a}^\dagger\hat{\rho} &\leftrightarrow (\alpha^* - \tfrac{1+s}{2}\tfrac{\partial}{\partial\alpha})F_s(\alpha)\\
\hat{\rho}\hat{a}^\dagger &\leftrightarrow (\alpha^* + \tfrac{1-s}{2}\tfrac{\partial}{\partial\alpha})F_s(\alpha)\\
\hat{a}\hat{\rho} &\leftrightarrow (\alpha + \tfrac{1-s}{2}\tfrac{\partial}{\partial\alpha^*})F_s(\alpha)\\
\hat{\rho}\hat{a} &\leftrightarrow (\alpha - \tfrac{1+s}{2}\tfrac{\partial}{\partial\alpha^*})F_s(\alpha)
\end{aligned} \tag{2.13}$$

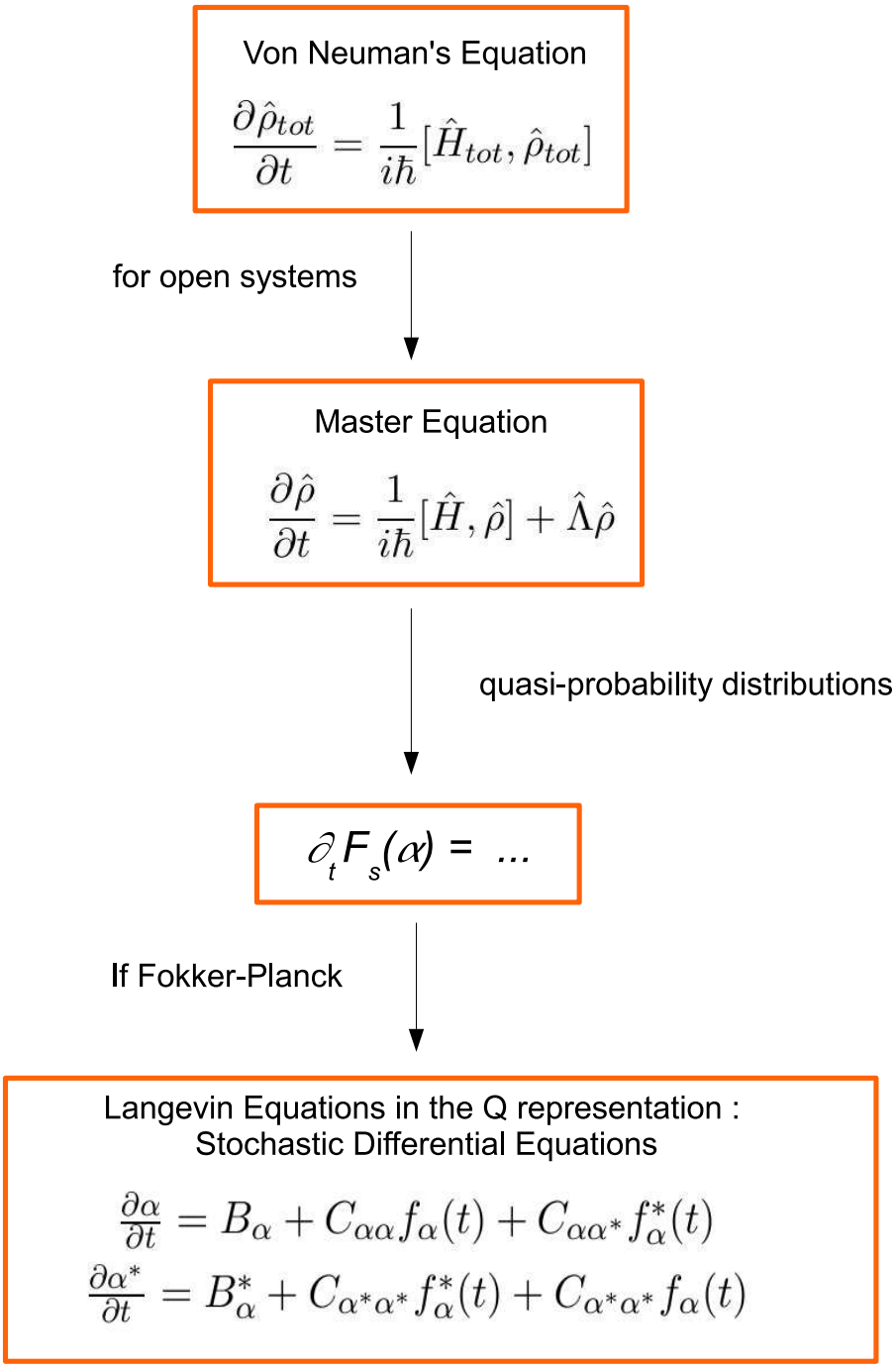

Figure 2.2: Brief description of the steps to obtain Langevin equations from a Master equation.

where, as we did for the characteristic function (Eq. 1.95), $s = +1$ corresponds to the P representation (thus $F_{+1}(\alpha) = P(\alpha)$) and $s = -1$ corresponds to the Q representation (so thus $F_{-1}(\alpha) = Q(\alpha)$).

As an example of how the correspondences between quantum operators and functions in the phase-space are obtained, we develop the steps to achieve the first one of the Eqs. (2.13). When applying the creation operator on a coherent state multiplied by the factor $e^{1/2|\alpha|^2}$ one realizes:

$$\hat{a}^\dagger e^{1/2|\alpha|^2}|\alpha\rangle = \sum_n \frac{\alpha^n}{\sqrt{n!}}\sqrt{n+1}|n+1\rangle = \frac{\partial}{\partial\alpha}(e^{1/2|\alpha|^2}|\alpha\rangle) \tag{2.14}$$

and similarly:

$$\langle\alpha|e^{1/2|\alpha|^2}\hat{a} = \frac{\partial}{\partial\alpha^*}(e^{1/2|\alpha|^2}\langle\alpha|). \tag{2.15}$$

Using the P representation for $\hat{\rho}$ (Eq. 1.78):

$$\hat{\rho} = \int d^2\alpha P(\alpha)|\alpha\rangle\langle\alpha|$$

we find:

$$\hat{a}^\dagger\hat{\rho} = \int d^2\alpha P(\alpha)\Big(\alpha^* + \frac{\partial}{\partial\alpha}\Big)|\alpha\rangle\langle\alpha|e^{|\alpha|^2} \tag{2.16}$$

and integrating by parts:

$$\hat{a}^\dagger\hat{\rho} = \int d^2\alpha|\alpha\rangle\langle\alpha|e^{|\alpha|^2}\Big(\alpha^* - \frac{\partial}{\partial\alpha}\Big)P(\alpha). \tag{2.17}$$

By inspection of the equation for $\hat{\rho}$, we can thus make a correspondence between $\hat{a}^\dagger$ and $\alpha^* - \frac{\partial}{\partial\alpha}$ and, similar formulas hold for the Q representation.

To obtain a complex equation we substitute the F_s representation for $\hat{\rho}$ into the Master equation (Eq. 2.4) and use the operator correspondences, leading an equation of the form:

(2.18)
$$\begin{gathered}\tfrac{\partial}{\partial t}F_s = -\tfrac{\partial}{\partial\alpha}A_\alpha F_s - \tfrac{\partial}{\partial\alpha^*}A_{\alpha^*}F_s + \\ +\tfrac{1}{2}\tfrac{\partial^2}{\partial\alpha^2}D_{\alpha\alpha}F_s + \tfrac{1}{2}\tfrac{\partial^{*2}}{\partial\alpha^{*2}}D_{\alpha^*\alpha^*}F_s + \tfrac{\partial^2}{\partial\alpha\partial\alpha^*}D_{\alpha\alpha^*}F_s + \tfrac{\partial^3}{\partial\alpha^3}J_{\alpha\alpha\alpha}F_s + \tfrac{\partial^3}{\partial\alpha^2\partial\alpha^*}J_{\alpha\alpha\alpha^*}F_s + ...\end{gathered}$$

where A_i, D_{ij} and J_{ijk} functions of α and α^*. Hereby we consider the case in which, for some s, the former equation reduces to:

$$\frac{\partial}{\partial t}F_s = -\frac{\partial}{\partial\alpha}A_\alpha F_s - \frac{\partial}{\partial\alpha^*}A_{\alpha^*}F_s + \frac{1}{2}\frac{\partial^2}{\partial\alpha^2}D_{\alpha\alpha}F_s + \frac{1}{2}\frac{\partial^{*2}}{\partial\alpha^{*2}}D_{\alpha^*\alpha^*}F_s + \frac{\partial^2}{\partial\alpha\partial\alpha^*}D_{\alpha\alpha^*}F_s \tag{2.19}$$

with a positive definite matrix D. This is a Fokker-Planck equation where the first derivative terms are called drift terms and A is the drift vector while the second derivative terms are the diffusion terms and D is the diffusion matrix. The main property of Fokker-Planck

equation is its relation with stochastic differential equations, because any Fokker-Planck equation can be mapped into a set of equivalent Langevin equations ([Zambrini]):

$$\begin{array}{c} \frac{\partial \alpha}{\partial t} = B_\alpha + C_{\alpha\alpha} f_\alpha(t) + C_{\alpha\alpha^*} f^*_\alpha(t) \\ \frac{\partial \alpha^*}{\partial t} = B^*_\alpha + C_{\alpha^*\alpha^*} f^*_\alpha(t) + C_{\alpha^*\alpha^*} f_\alpha(t) \end{array} \tag{2.20}$$

with f_i white Gaussian noise. The importance of the Langevin equations lies in the possibility of performing numerical simulation of these stochastic equations for general complicated drift and diffusion terms. In fact this method is used in this Master thesis.

2.2.1 PCOPO Langevin equations in the Q representation

The methodology summarized in Fig. 2.2 applies successfully in the linear regimes but the presence of non-linearities leads to a functional differential equation for the quasi-probability that generally is not Fokker-Planck like. In a OPO described by the (multi-mode) Hamiltonian, Eq. (2.6) the offending term is the interaction term (Eq. 2.9) such that:

$$[\hat{A}_0(x)\hat{A}_1^{\dagger^2}(x) + h.c., \hat{\rho}] \Longleftrightarrow (s\alpha_0 \frac{\delta^2}{\delta\alpha_1^2} + \frac{1-s^2}{4}\frac{\delta^3}{\delta\alpha_1^2\delta\alpha_0^*} + \frac{\delta}{\delta\alpha_0}\alpha_1^2 - 2\alpha_0\alpha_1^*\frac{\delta}{\delta\alpha_1} + c.c.)F_s.$$

In the Q representation (s=-1) this equation suffers of negative diffusion, although Q is always positive and well-behaved. It can be shown ([Zambrini & al. (03)]) that the evolution equation of the functional Q for an OPO is:

$$\begin{array}{l} \frac{\partial Q(\alpha_0,\alpha_1)}{\partial t} = \int d^2x \left\{ -\left(\frac{\delta}{\delta\alpha_0(x)} V_0 + \frac{\delta}{\delta\alpha_1(x)} V_1 + c.c. \right) \right. \\ + \int d^2x' \left[2\gamma_0 \frac{\delta^2}{\delta\alpha_0(\vec{x})\delta\alpha_0^*(x')} + 2\gamma_1 \frac{\delta^2}{\delta\alpha_1(x)\delta\alpha_1^*(x')} + \right. \\ \left. \left. \frac{1}{2}\left(-g\alpha_0 \frac{\delta^2}{\delta\alpha_1(x)\delta\alpha_1(x')} + c.c \right) \right] \right\} Q(\alpha_0,\alpha_1), \end{array} \tag{2.21}$$

where the drift terms are

$$V_0 = -\gamma_0[(1+i\Delta_0) - ia_0\nabla^2]\alpha_0(x,t) - \frac{g}{2}\alpha_1^2(x,t) + E \tag{2.22}$$

$$V_1 = -\gamma_1[(1+i\Delta_1) - ia_1\nabla^2]\alpha_1(x,t) + g\alpha_0(x,t)\alpha_1^*(x,t). \tag{2.23}$$

If the diffusion term is positive, then our evolution equation is a well-defined Fokker-Planck equation. In the other case this equation does not describe an ordinary diffusion process. For equation (2.21) the diffusion term is positive if

$$|\alpha_0(\vec{x},t)| < \frac{2\gamma_1}{g}. \tag{2.24}$$

The modulus of the stationary field at threshold takes the value $|A_0^{thr}| = \gamma_1/g$ (see section 2.3). This means that the condition given in the inequality (2.24) corresponds to pump trajectories taking values that are less than twice the threshold value. Staying in a region far from the limit (2.24) an extremely large fluctuation in a trajectory would be necessary in order to lose the positiveness of the diffusion. Clearly these trajectories have a negligible probability to appear, and never appeared in our simulations. For these reasons, the approximation we use, following [Zambrini & al. (03)] is to study Langevin equations related to the Fokker-Planck equation given by (2.21) and (2.24), neglecting any trajectories that would make negative the diffusion term. Clearly the condition (2.24) does not depend on the frequency at which the system is pumped. For this reason the method is suitable, and has been already successfully used, to describe non-linear fluctuations in stripe patterns in Second Harmonic Generation in a regime of pump values limited by Eq. (2.24) [Bache & al.].

From Eqs.(2.21-2.24), with the scaling

$$\gamma_0 = \gamma_1 = \gamma \ , \quad a_0 = a_1/2 = a, \tag{2.25}$$
$$t' = \gamma t \ , \quad x' = \frac{x}{\sqrt{a}},$$
$$A_i' = \frac{g}{\gamma} A_i \ , \quad E' = \frac{g}{\gamma^2} E \tag{2.26}$$

we obtain the equations for the pump α_0 and the signal α_1 fields:

$$\partial_t \alpha_0(x,t) = -\left[1 + i\Delta_0 - i\nabla^2\right] \alpha_0(\vec{x},t) + E - \frac{1}{2}\alpha_1^2(x,t) + \sqrt{\frac{2}{a}}\frac{g}{\gamma}\xi_0(x,t) \tag{2.27}$$

$$\partial_t \alpha_1(\vec{x},t) = -\left[1 + i\Delta_1 - 2i\nabla^2\right] \alpha_1(\vec{x},t) + \alpha_0(x,t)\alpha_1^*(x,t) + \sqrt{\frac{2}{a}}\frac{g}{\gamma}\xi_1(x,t). \tag{2.28}$$

The first term on the right side represent the losses and the following one the detuning (i.e. the difference between the frequency of the corresponding field and the closest natural one of the cavity). The effect of the modulation of the refractive index in the transverse profile due to the photonic crystal, $n = n(x)$, lead to detuning of the pump and signal also modulated:

$$\begin{aligned} \Delta_0 &\to \Delta_0 + M_0 \sin k_{pc} x \\ \Delta_1 &\to \Delta_1 + M_1 \sin k_{pc} x. \end{aligned} \tag{2.29}$$

The Laplacian models the diffraction term. The parameter a is defined as $a = 1/2\pi TF$, where $F = \frac{b^2}{\lambda L}$ is the Fresnel number. In the pump equation appears the injected laser field E. Then, in both, pump and signal equation appears the coupling terms due to the multimode treatment and the non linearities of our system, Eq. (2.9). Finally, due to the presence of diagonal terms in the diffusion matrix of Eq. (2.21), we have a *phase sensitive*

white noise:

$$\xi_1(x,t) = \left[\frac{-\alpha_{0I}(x,t)}{2\sqrt{2+\alpha_{0R}(x,t)}} + \frac{i}{2}\sqrt{2+\alpha_{0R}(x,t)}\right]\phi(x,t) + \sqrt{\frac{1-\frac{|\alpha_0(x,t)|^2}{4}}{2+\alpha_{0R}(x,t)}}\psi(x,t) \tag{2.30}$$

with $\alpha_0 = \alpha_{0R} + i\alpha_{0I}$ and ϕ, ψ and with non-vanishing moments:

$$\langle \xi_0(x,t)\xi_0^*(x',t')\rangle = \delta(x-\vec{x'})(t-t') \tag{2.31}$$

$$\langle \phi(x,t)\phi^*(x',t')\rangle = \delta(x-x')(t-t') \tag{2.32}$$

$$\langle \psi(x,t)\psi^*(x',t')\rangle = \delta(x-x')(t-t'). \tag{2.33}$$

We observe that the noise is multiplicative, with moments of the signal noise depending on the value of the pump field. However due to the form of $\hat{H}$ (quadratic in $\hat{A}_1$ and linear in $\hat{A}_0$), these equations have the same formal expression in the Ito or Stratonovich interpretations [Gardiner]. The moments (2.32) and (2.33) fix only three of the four degrees of freedom in the choice of the real and imaginary parts of the noise term ξ_1; this depends on the multiplicity of Langevin processes associated with the same Fokker-Planck equation [Gardiner]. We solve these Langevin equations by numerical simulation. Trajectories that do not satisfy the condition (2.24) never appeared in the regimes we consider.

2.3 PCOPO deterministic classical equations

The Eqs. (2.27,2.28) describe the time evolution of the pump $\alpha_0(x,t)$ and signal $\alpha_1(x,t)$ fields treated as complex functions and giving exactly the moments of the bosonic operators $\hat{A}_0(x,t)$ and $\hat{A}_1(x,t)$. There are analogous equations for the classical fields and are deterministic, in the sense that they do not have noise terms so, there are not fluctuations. The model can be derived in a rigorous way from the classical Maxwell-Bloch for the intracavity electromagnetic field equations by the introduction of some standard conditions as the mean field ans the slowly varying envelopes [Lugiato & al.]. The mean field limit, which implies $T << 1$, reduces the dynamics to a single mode propagating in z with wavelength ω (the closest possible to the natural frequency of the cavity), and make suitable the adiabatic elimination of the atomic variables. About the slowly varying envelope, the injected laser can be consider a coherent monochromatic light. However, we are interested in the transverse profile of the pump and signal fields so we assume they are quasi-monochromatic beams of the form:

$$f(x,y,z,t)e^{i(k_z z-\omega_0 t)} \tag{2.34}$$

where the exponential term accounts for a plane wave moving along the z direction, thus we assume the dependence of f on z and t is slow:

$$|\partial_z f| << k_z|f| \tag{2.35}$$

$$|\partial_t f| << \omega_0|f| \tag{2.36}$$

so we neglect the terms involving the derivatives of the amplitude. Because $T << 1$ we want a to be of order of unity, we assume large Fresnel numbers, $F >> 1$. It is also assumed small diffraction angles, valid whenever the transverse wave vectors components $\vec{k}_\perp = (k_x, k_y)$ of the propagating fields are small with respect to the longitudinal component k_z. This is called the paraxial approximation.
The deterministic equations for classical pump $\mathcal{A}_0(x,t)$ and signal $\mathcal{A}_1(x,t)$ are then:

$$\partial_t\mathcal{A}_0(x,t) = -\left[1 + i(\Delta_0 + M_0 \sin k_{pc}x) - i\nabla^2\right]\mathcal{A}_0(\vec{x},t) + E - \frac{1}{2}\mathcal{A}_1^2(x,t) \tag{2.37}$$

$$\partial_t\mathcal{A}_1(\vec{x},t) = -\left[1 + i(\Delta_1 + M_1 \sin k_{pc}x) - 2i\nabla^2\right]\mathcal{A}_1(\vec{x},t) + \mathcal{A}_0(x,t)\mathcal{A}_1^*(x,t). \tag{2.38}$$

Then these equations can be obtained averaging Eqs. (2.27,2.28), where $\mathcal{A}_0 = \langle\alpha_0\rangle$ and $\mathcal{A}_1 = \langle\alpha_1\rangle$, one we assume that higher order moments factorize ($\langle\alpha_1^2\rangle = \langle\alpha_1\rangle^2$ for instance). Now we consider the **OPO without photonic crystal** in order to show where the critical wave number comes from and to establish the procedure we perform for the study of the bifurcation diagram in the OPO with photonic crystal (Chapter 3). Following [Oppo & al. (94)], we look for stationary solutions (independent on t) and uniform (independent on x) of Eqs. (2.37,2.38):

$$0 = -\left[(1 + i\Delta_0) - i\nabla^2\right]\mathcal{A}_0^{st} + E - \frac{1}{2}\mathcal{A}_1^{st\ 2} \tag{2.39}$$

$$0 = -\left[(1 + i\Delta_1) - 2i\nabla^2\right]\mathcal{A}_1^{st} + \mathcal{A}_0^{st}\mathcal{A}_1^{st\ *} \tag{2.40}$$

There is a trivial solution:

$$\mathcal{A}_0^{st} = \frac{E}{1 + i\Delta_0}; \qquad \mathcal{A}_1^{st} = 0 \tag{2.41}$$

and another:

$$\mathcal{A}_0^{st} = \frac{E(i + \Delta_1)}{(i + \Delta_1)(i + \Delta_0) + |\mathcal{A}_1 st|^2/2}; \qquad \mathcal{A}_1^{st} = \pm\sqrt{\frac{E|\mathcal{A}_1 st|^2}{(i + \Delta_1)(i + \Delta_0) + |\mathcal{A}_1 st|^2/2}} \tag{2.42}$$

In order to study the stability of these solutions linearization around them is performed. Hereby we just present the trivial solution case, linearizing around the stationary state 2.41:

$$\mathcal{A}_0(x,t) = \mathcal{A}_0^{st} + \delta\mathcal{A}_0(x,t); \qquad \mathcal{A}_1(x,t) = \delta\mathcal{A}_1(x,t) \tag{2.43}$$

We rewrite the equations for these fluctuations and by neglecting the non linear terms in the fluctuations we find that the equations for the pump and the signal fields are decoupled. The eigenvalues for the Fourier modes are:

$$\lambda_0 = -1 - i(k^2 + \Delta_0) \qquad \lambda_{1,2} = -1 \pm \sqrt{|\mathcal{A}_0^{st}|^2 - (\Delta_1 + 2k^2)^2} \tag{2.44}$$

It is well known that a negative (real part of an) eigenvalue means the state is stable while a positive (real part) means instability. By observing our eigenvalues, it is clear that the detuning of the pump Δ_0 does not play any role and that only λ_1 may change sign, giving us the stability threshold for the driving laser field E at pump frequency (substituting Eq.2.41):

$$E^{thr} = \sqrt{(1 + \Delta_0^2)[1 + (\Delta_1 + 2k^2)^2]}. \tag{2.45}$$

We see that:

- when $\Delta_1 \geq 0$ the minimum is $k = 0$ and it means the signal arises as a plane wave. These values of the signal detuning give place to a multistabilty regime.
- when $\Delta_1 < 0$ because the minimum energy is obtained at:

  $$|k| = \sqrt{\frac{-\Delta_1}{2}} \tag{2.46}$$

  and the signal forms a stripe pattern with $k = k_c$. Therefore with negative signal detuning there is spontaneous pattern formation.

Bifurcation diagrams are plotted in Chapter 3 showing the stability of the solutions. Here it is important to stress that pattern formation threshold and parametric threshold coincide for negative signal detuning.
In the following chapter we will consider the case of the PCOPO. At difference to the case reviewed here (in absence of photonic crystal), the stationary state will be generally not homogeneous ans semi-classical results have been obtained by Dr. D. Gomila.

3

Spatial Instabilities in PCOPO

We have seen in the introduction that pattern formation has been intensively studied in the last decades, also in OPOs. The possibility of optical pattern inhibition using photonic crystals has been recently proposed by considering a Kerr cavity and a singly-resonant OPO [Gomila & al. (03)], [Gomila & al. (04)]. In these works it was shown the spatial instability thresholds move to larger values of the pump for appropriate modulation of the photonic crystal. This theoretical prediction has been recently confirmed in two experiments in vertical-cavity surface emitting laser [Marsal & al.] (this result is reproduced in Fig. 3.1) and with a photorefractive medium in single-mirror feedback configuration [Terhalle & al.]. The inhibition of spatial instability arises because the modes of the pattern falls within the band gap of the photonic crystal.

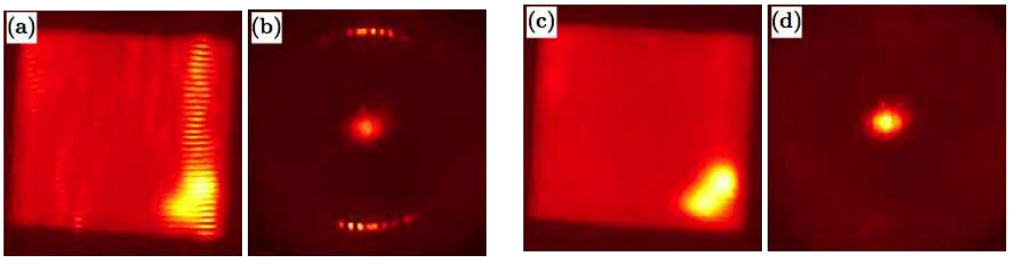

Figure 3.1. Experimental results confirming the spatial instabilities inhibition by using photonic crystals [Marsal & al.]. a) A horizontal stripes pattern is formed in the real space (near field) in the transverse profile (x, y). b) The Fourier transform of the pattern is represented in the far field (k_x, k_y), where the spatial modes k and $-k$ are shown (with some distorsion due to the lens geometry) and in the center the homogeneous component ($k = 0$) appears. c) When a modulation in the transverse profile is included in the system the pattern in the near field does not appear anymore. d) In the far field, only the homogeneous component is found.

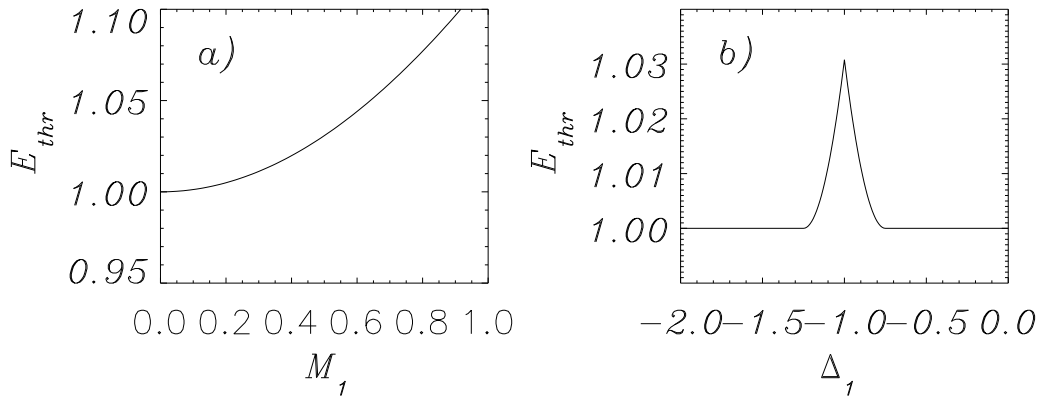

Figure 3.2. Instability thresholds in singly-resonant degenerate OPO for parameters such that the pump threshold in absence of the photonic crystal is 1. These results are the representation of the analytical solutions given in [Gomila & al. (04)]. a) Threshold inhibition for modulation of the signal refractive index with amplitude M_1 and wavenumber twice the critical one. b) Pump threshold as a function of the averaged detuning.

Apart from the interest from the fundamental point of view, the use of photonic crystal allows to control the transverse properties of emitted light avoiding unwanted spatial instabilities that often spoil the quality of the beam in broad are non linear optical devices. In this chapter we show the role of photonic crystals in a type I Degenerate Optical Parametric Oscillator with photonic crystal (PCOPO) focusing on the classical equations. The intracavity photonic crystal is modelled by spatial dependent detunings that can have different contrast or amplitudes for pump and signal fields M_0 and M_1, respectively. We remind here the deterministic equations for the pump $\mathcal{A}_0$ and for the signal $\mathcal{A}_1$ introduced in the Chapter 2, Eqs. (2.37) and (2.38):

$$(3.1)\quad \partial_t \mathcal{A}_0(x,t) = -\left[1 + i(\Delta_0 + M_0 \sin k_{pc} x) - i\nabla^2\right] \mathcal{A}_0(x,t) + E - \frac{1}{2}\mathcal{A}_1^2(x,t)$$

$$(3.2)\quad \partial_t \mathcal{A}_1(x,t) = -\left[1 + i(\Delta_1 + M_1 \sin k_{pc} x) - 2i\nabla^2\right] \mathcal{A}_1(x,t) + \mathcal{A}_0(x,t)\mathcal{A}_1^*(x,t).$$

The spatial modulation of the detuning, modeling the photonic crystal, in general forbids the existence of homogeneous trivial stationary solutions, like Eq. (2.41) in section 2.3. Still, the vanishing signal solution is always present and some analytical results can be obtained restricting the stability analysis to the most intense spatial harmonics. This method was used in [Gomila & al. (04)] in the case of a singly-resonant degenerate OPO and the analytically obtained threshold is shown in Fig. 3.2.

The mentioned pattern inhibition takes place and the threshold in this case is always increased with respect to the well known case without photonic crystal, whose value is $E_{thr} = 1$. The photonic crystal has, therefore, the effect of inhibiting the spatial instability as well as the parametric emission. Inhibition was also observed in the case of a cubic

instead of a quadratic non-linearity, suggesting that this is a general effect of photonic crystals. We find, however, that this is not always the case, as discussed in the following sections.

3.1 Stationary solutions and linear stability analysis

As anticipated before, even in presence of spatial modulation due to the photonic crystal ($M_0 \neq 0$ and/or $M_1 \neq 0$) the vanishing stationary solution for the signal field:

$$\mathcal{A}_1^{st} = 0 \tag{3.3}$$

always exists. However, there is not homogeneous stationary solution for the pump field whenever the photonic crystal influence the pump detuning $M_0 \neq 0$.
The stationary pump solution fulfills the equation:

$$(1 + iD_0(x) - i\nabla^2)\mathcal{A}_0^{st}(x) = E. \tag{3.4}$$

If $M_0 \neq 0$, that is, in absence of photonic crystal influencing the pump mode, $D_0 = \Delta_0$ ans we still have the spatially homogeneous steady solution, as Eq. (2.41):

$$\mathcal{A}_0^{st} = \frac{E}{1 + i\Delta_0}. \tag{3.5}$$

On the other hand for $M_0 \neq 0$ we have:

$$D_0(x) = \Delta_0 + M_0 \sin(k_{pc}x) \tag{3.6}$$

and there is not homogeneous solution for the equation:

$$(1 + i\Delta_0 + iM_0 \sin(k_{pc}x) - i\nabla^2)\mathcal{A}_0^{st}(x) = E. \tag{3.7}$$

By defining the Fourier transform as:

$$\mathcal{A}_{0,1}(x,t) = \int \frac{dk}{\sqrt{2\pi}} \int \frac{d\omega}{\sqrt{2\pi}} e^{i(kx-\omega t)} \mathcal{A}_{0,1}(k,\omega) \tag{3.8}$$

$$\mathcal{A}_{0,1}^*(x,t) = \int \frac{dk}{\sqrt{2\pi}} \int \frac{d\omega}{\sqrt{2\pi}} e^{i(kx-\omega t)} \mathcal{A}_{0,1}^*(-k,-\omega) \tag{3.9}$$

Eq. (3.7) becomes:

$$(1 + i\Delta_0 + ik^2)\mathcal{A}_0^{st}(k) + \frac{M_0}{2}\left(\mathcal{A}_0^{st}(k - k_p) - (\mathcal{A}_0^{st}(k + k_p)\right) = E\delta(k). \tag{3.10}$$

We see that each mode k is coupled to the shifted ones $\pm k$. Considering:

$$k = nk_{pc} \tag{3.11}$$

with n integer, we obtain a chain of equations:

$$(1 + i\Delta_0 + in^2k_{pc}^2)\mathcal{A}_0^{st}(nk_{pc}) + \frac{M_0}{2}\big(\mathcal{A}_0^{st}((n-1)k_{pc}) - (\mathcal{A}_0^{st}((n+1)k_{pc})\big) = E\delta_{n0}. \tag{3.12}$$

Equations for n, $n+1$ and $n-1$ are coupled. We truncate the hierarchy by introducing the approximation to neglect spatial harmonics higher than the first in the expansion of the steady state. In other words, we consider only $k = 0, \pm k_{pc}$:

$$\mathcal{A}_0^{st}(x) = \sum_{n=+\infty}^{n=-\infty} \mathcal{A}_0^{(n)} e^{ik_{pc}nx} \simeq \mathcal{A}_0^{(0)} + \mathcal{A}_0^{(1)} e^{ik_{pc}x} + \mathcal{A}_0^{(-1)} e^{-ik_{pc}x} \tag{3.13}$$

Then we obtain a hierarchy of 3 coupled equations for $n = \{0, \pm 1\}$:

$$n = 0 \;\rightarrow\; (1 + i\Delta_0)\mathcal{A}_0^{st}(0) + \tfrac{M_0}{2}(\mathcal{A}_0^{st}(-k_{pc}) - \mathcal{A}_0^{st}(k_{pc}) = E$$

$$n = 1 \;\rightarrow\; (1 + i\Delta_0 + ik_{pc}^2)\mathcal{A}_0^{st}(k_{pc}) + \tfrac{M_0}{2}\mathcal{A}_0^{st}(0) = 0 \tag{3.14}$$

$$n = -1 \;\rightarrow\; (1 + i\Delta_0 + ik_{pc}^2)\mathcal{A}_0^{st}(-k_{pc}) - \tfrac{M_0}{2}\mathcal{A}_0^{st}(0) = 0.$$

Here we present the solution under the assumption:

$$\Delta_0 = 0 \tag{3.15}$$

leading to the algebraically simpler expressions:

$$\mathcal{A}_0^{st}(0) = \frac{E(1 + ik_{pc}^2)}{(1 + ik_{pc}^2) + \frac{M_0^2}{2}}; \qquad \mathcal{A}_0^{st}(k_{pc}) = -\mathcal{A}_0^{st}(-k_{pc}) = \frac{-\frac{M_0}{2}E}{(1 + ik_{pc}^2) + \frac{M_0^2}{2}}. \tag{3.16}$$

Linearized equations for *signal* perturbations around the steady state are decoupled from the linearized *pump* equations, similarly to the case of the OPO without photonic crystal (section 2.3). The linear stability analysis, however, is modified not only by the presence of the detuning modulation (like in [Gomila & al. (03)]) but also by the spatial coupling between modes due to the modulation of the reference state, as discussed in the next section. The photonic crystal enters as modulation of the detuning $\Delta_1(x)$ and also for the modulation in the steady solution ($\mathcal{A}_0^{st} = \mathcal{A}_0^{st}(x)$). When we linearize the signal field around the steady solution the following equation for the signal fluctuations is obtained:

$$\partial_t \delta\mathcal{A}_1(x,t) = -\left[1 + i(\Delta_1 + M_1 \sin k_{pc}x) - 2i\nabla^2\right]\delta\mathcal{A}_1(x,t) + \mathcal{A}_0^{st}(x)\delta\mathcal{A}_1^*(x,t) \tag{3.17}$$

In the following we will keep the assumption of vanished pump detuning, Eq. 3.15, and negative signal detuning.

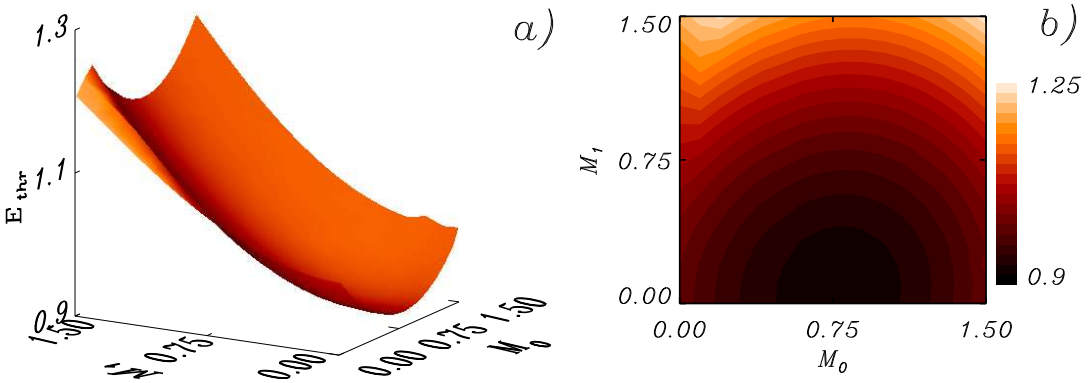

Figure 3.3. a) Pump threshold E_{thr} as a function of the amplitude of the modulation in the pump M_0 and in the signal M_1 for the case $k_{pc} = 2k_c$. Throughout this section we take $\Delta_0 = 0$ and $\Delta_1 = -1$. For these parameter values $k_{pc} = \sqrt{2}$. b) Projection over the M_0, M_1 plane with the same color scale.

3.1.1 Case with critical signal mode in the center of the band gap

The most promising case, inspired by [Gomila & al. (03)], is obtained for photonic crystal bandgap at the wavelength that would become unstable at threshold in absence of photonic crystal. Then, we start considering Eq. (1.8). for $k = k_c$, that is:

$$k_{pc} = 2k_c. \tag{3.18}$$

We stress that k_c is the wave number that would be unstable without photonic crystal. The predicted instability threshold is represented in Fig. 3.3 and 3.4. We see that, depending on the contrast M_0 and M_1 introduced by the photonic crystal, the threshold value for the pump to give rise down conversion moves to values different from 1. In Fig. 3.4 we see that the effect of the photonic crystal is not the same in the pump and in the signal fields. The case of modulation only in the signal, ($M_0 = 0$), has stability analysis identical to what presented in [Gomila & al. (04)]. Only inhibition of pattern formation and of the associated down-conversion is found, Fig 3.4b. The photonic crystal fast modulation inhibits the instability at the critical wavelength. The pump mode remains homogeneous below threshold and its fluctuations are linearly decoupled from the signal. The main novelty is for $M_0 \neq 0$: the photonic crystal changes the spatial profile of the pump, introducing a modulation similar to the one appearing in an OPO above threshold without any photonic crystal. In fact all the harmonics of k_{pc} are present. Looking at the linearized equation for the signal fluctuations Eq. 3.17, we see that the effect of the photonic crystal is similar to inject the device with a spatially modulated pump. This induces instability for pump E lower than without photonic crystal. The pattern seems to be stimulated by this modulation in the pump and this allow to lower the OPO threshold

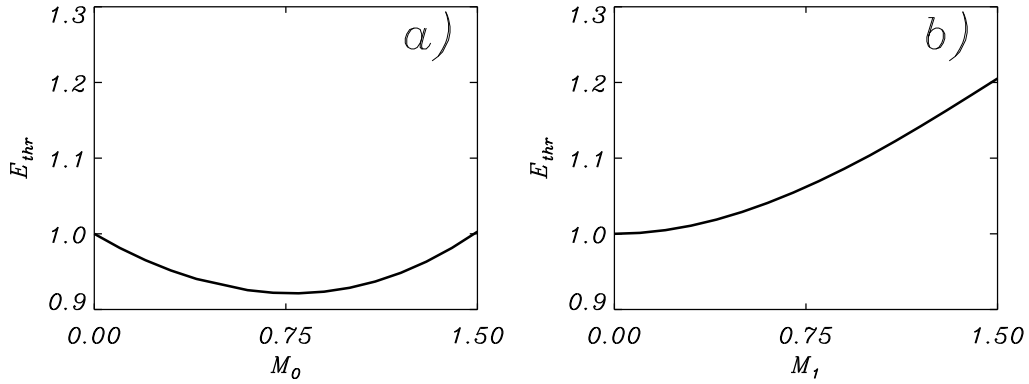

Figure 3.4. Pump threshold E_{thr} for the case $k_{pc} = 2k_c$ as a function of the amplitude of the modulation in the pump M_0 with $M_1 = 0$, (a), and in the signal M_1 with $M_0 = 0$, (b), resulting from two cuts of the Fig. 3.3a. The case of modulation only in the pump gives rise to an unexpected lowering of the threshold.

below the standard operation value $E = 1$. Until now we have found that the threshold can be decreased a 10% by the use of a photonic crystal.

3.1.2 Case with signal critical mode out of the band gap

We consider now:

$$k_{pc} = k_c. \tag{3.19}$$

where, as usually, k_c is the critical wavenumber that would become unstable at threshold without photonic crystal. In this case, only inhibition of pattern formation and of the associated down-conversion is found but is stronger than in the case considered in the previous section. For modulation only in the signal detuning at the critical wave-length we see that the stability of the system is almost unchanged, Fig. 3.6b. Looking at the dispersion relation, we could actually say that its expression is almost unchanged because now the photonic crystal introduces only intramodal couplings between different transverse k (for instance $\mathcal{A}_1^{st}(k_c)$ due to the photonic crystal is coupled with $\mathcal{A}_1^{st}(2k_c)$ and $\mathcal{A}_1^{st}(0)$) that have no gain (the coupled mode with gain is $\mathcal{A}_1^{s*}(-k_c)$). The fact that, for $M_0 = 0$ for photonic crystal periodicity similar to k_c, the effect of pattern inhibition whose very weak was already reported in [Gomila & al. (04)] (see also Fig. 3.2b). We consider now what happens if also the pump is influenced by the photonic crystal ($M_0 \neq 0$). Then the modulation is at the k_c so all the spatial harmonics are present into the pump solution and not only the even ones. The inhibition is really strong with respect to the case of $k_{pc} = 2k_c$, even for photonic crystal modulations not too high. This is quite sparingly, as we actually see that now the instability inhibition is even larger that in Fig. 3.4b. Looking at the linearized equation for the signal we see that in this case the instability at $k_c = k_{pc}$ can

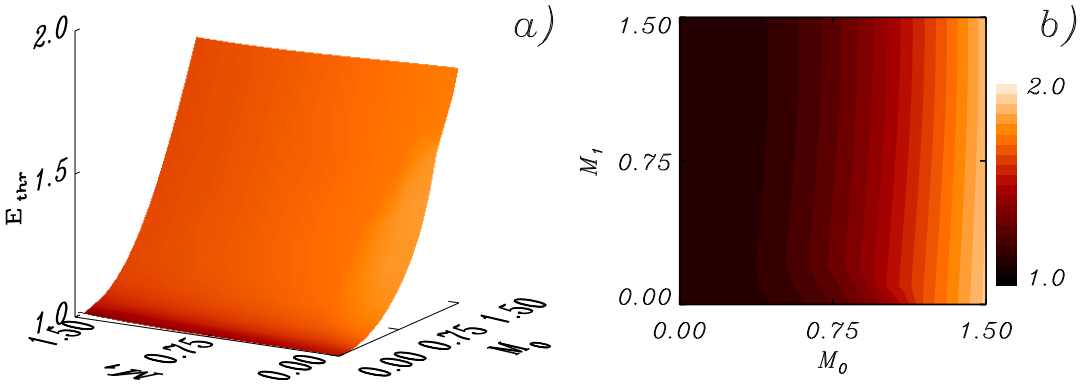

Figure 3.5. a) Pump threshold E_{thr} as a function of the amplitude of the modulation in the pump M_0 and in the signal M_1 for the case $k_{pc} = k_c$. Throughout this section we take $\Delta_0 = 0$ and $\Delta_1 = -1$. For these parameter values $k_{pc} = \sqrt{2}$. b) Projection over the M_0, M_1 plane with the same color scale.

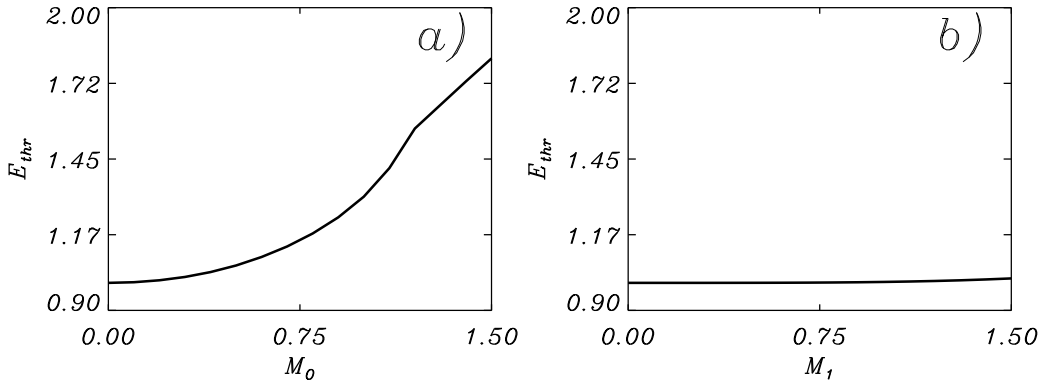

Figure 3.6. Pump threshold E_{thr} for the case $k_{pc} = k_c$ as a function of the amplitude of the modulation in the pump M_0 with $M_1 = 0$, (a), and in the signal M_1 with $M_0 = 0$, (b), resulting from two cuts of the Fig. 3.5a. Throughout this section we take $\Delta_0 = 0$ and $\Delta_1 = -1$. The case of modulation only in the pump mode reproduce the results given in [Gomila & al. (04)], where only inhibition of the pattern formation was achieved.

be described by an equation similar to the one obtained without photonic crystal because the higher harmonics in the pump do not couple significantly to the signal. We can say that the most important spatial harmonics of the pump ($\mathcal{A}_0^{st}(Nk_{pc})$) do not couple with the signal most unstable wave-number $\mathcal{A}_1^{st}(k_{pc})$. We will see the only important effect of the pump modulation is the introduction of an effective detuning, that increases the threshold.

3.2 Efficiency

We consider now the intensity of the arbitrary state in different spatial modes in order to see how energy is transferred between them and also the efficiency of the down conversion

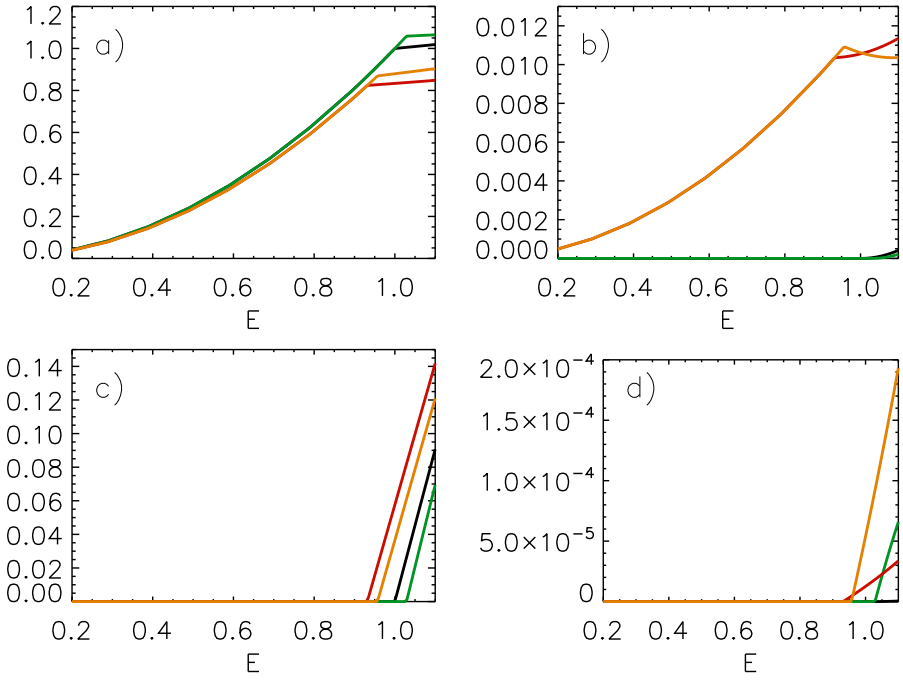

Figure 3.7. Bifurcation diagrams of pump and signal field with the injected field threshold as control parameter for $k_{pc} = 2k_c$. a) $|\mathcal{A}_0(0)|$, b)$|\mathcal{A}_0(2k_c)|$, c) $|\mathcal{A}_1(k_c)|$, and d) $|\mathcal{A}_1(3k_c)|$ for different configurations of the photonic crystal. Black: without photonic crystal, i.e. $M_0 = M_1 = 0$ with threshold at $E = 1$; green: $M_0 = 0, M_1 = 0.5$ with threshold at $E = 1.029$; red: $M_0 = 0.5, M_1 = 0$ with threshold at $E = 0.932$ and orange: $M_0 = M_1 = 0.5$ with threshold at $E = 0.957$. Modulation of refractive index in the transverse profile does not change the efficiency of the Degenerate Parametric Down Conversion process $2\omega \rightarrow \omega + \omega$. The instabilities of the solution for the pump at $k = 0$ and for the signal at $k = k_c$ give rise to a bifurcation for the next harmonics, odd for the signal and even for the pump as $\omega_p = 2\omega_{signal}$ means $k_p = 2k_c$.

process. By plotting the pump and signal fields as functions of the input field E it is possible to visualize a bifurcation diagram, that depends on the presence and the different configurations of the photonic crystal. In Fig.3.7 the pump and the signal intensities are presented in different modes k. These curves are obtained by numerical simulation of Eqs. (2.37) and (2.38), and reaching the stationary solution. In fig. 3.7a the pump field is plotted for $k = 0$,corresponding to the homogeneous near field component receiving energy from the input E. It is seen that the stationary $\mathcal{A}_0^{st}(0)$ is almost unchanged when introducing the photonic crystal, being the most evident difference only the position of the instability threshold. In Fig. 3.7b we see that the pump $|\mathcal{A}_0^{st}(2k_c)|$ is intense in the cases in which the photonic crystal is inducing the modulation (that is for $M_0 \neq 0$), as expected. Comparing Fig. 3.7a and b below threshold we see that these cases (orange curve, for instance) the $2k_c$ mode is gaining momentum while the homogeneous of the pump is losing it. The efficiency in the signal generation represented in Fig. 3.7c does only depend on the effective distace from the threshold in each device configuration.

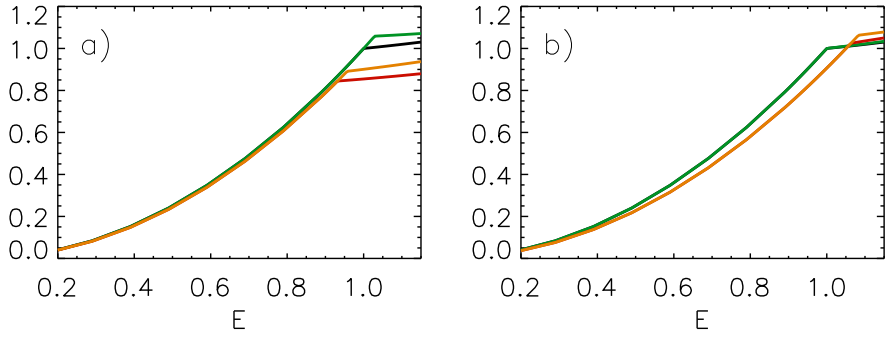

Figure 3.8. Intracavity energy numerically calculated as the sum of the complete set of squared absolute value of harmonics of the pump for the case: a) $k_p = 2k_c$ and b) $k_p = k_c$.

In other words, as a consequence of the change in the threshold described above, there is the expected change of efficiency in the signal production. For a fixed value of the pump E, say $E = 1.05$ (remember that without photonic crystal $E_{thr} = 1$) we obtain that the larger signal intensity appears for the PCOPO in which the instability threshold is most lowered (red curve in Fig.3.7a). All the signal curves in Fig.3.7c can be overlapped by a simple translation and we do not find qualitative changes in the bifurcation diagrams after introduction of photonic crystal.

Here we show numerical results corresponding to the case $k_{pc} = 2k_c$ but qualitative similar results are also found for $k_{pc} = k_c$, where the instabilities occurs for $E_{thr} \geq 1$ in all the photonic crystal configurations.

In order to clarify, if the modulation of the photonic crystal acts as an effective pump detuning that decreases the intracavity energy less input energy enters into the cavity explaining why the thresholds rise so much in this case giving the strongest pattern inhibition. We look now at the total energy entering into the system. That is:

$$U = \int |A_0(x)|^2 dx. \tag{3.20}$$

In Fig. 3.8a we see that for $k_{pc} = 2k_c$, and focusing below threshold, in all the cases there is almost the same energy in the system. This would be different for homogeneous pump detuning that would actually have the effect to reduce the energy coupling with the cavity (as clear from Eq. 3.5) which is in fact what occurs for $k_{pc} = k_c$, $M_0 \neq 0$, as it is shown in Fig 3.8b (red and orange curves).

3.3 Summary

In the case of optical parametric oscillators the inhibition of the instability also imply the possibility to control the parametric threshold (as they coincide). Due to the mixing of

two different frequencies in OPOs $(2\omega, \omega)$we find a diffrent scenario than in previously considered devices [Gomila & al. (04)]. The analysis of the PCOPOs in which the modulation appears in the pump detuning instead of the signal, or in both fields, shows a complex scenario. The threshold, for some parameters values, is found to be lowered by the presence of the photonic crystal, instead of being raised. It follows that threshold can be largely 'tuned', depending on the spatial modulation introduced by the photonic crystal. If the rise of the threshold is explained in terms of band gad inhibition or effective pump detuning (depending on the cases), its lowering is a novel effect and seems to be associated to a mechanism of stimulation of the pattern.

Besides, we analyzed the multimode character and efficiency of the process. The effect of the photonic crystal is just to shift the threshold but the efficiency for fixed distances from the threshold in the different cases is unchanged, at least until values of the injected pump 50% above the corresponding threshold.

4

Spatial Quantum Correlations in OPO with photonic crystal

The main body of the results presented in this chapter concerns the direct analysis of quantum fluctuations around the stationary state below threshold, within a linear approximation, as we described in Chapter 3. Numerical simulations of Eqs. (2.27,2.28) allow to characterize the spatio-temporal *dynamics* of the quantum light fields. In Fig. 4.1 we present a set of results of the near fields evolution and we see when the photonic crystal changes the shape of the stationary solution, in particular, below threshold. We notice that the stripe pattern spontaneously created above threshold is -in first approximation- unchanged with or without photonic crystal.

The quantum *correlations* of the quantum fields represented in Fig. 4.1 are calculated numerically. In particular, we focus here on the spatial distribution of quantum fluctuations and on correlations between opposite spatial modes. A previous work in an OPO without photonic crystal showed that these quantum correlations and squeezing where present not only below threshold (in quantum images), but also in presence of an intense signal field, above threshold [Zambrini & al. (03)]. Here we study their robustness or improvement in presence of a photonic crystal, and in this Master Thesis we focus on the below threshold regime.

4.1 Spatial Antibunching

Here we discuss the effect of the photonic crystal on quantum fluctuations both in the pump and in the signal light states. Non-classical features in the twin beams correlations are displayed for negative values of the normal-ordered variance of the difference of the

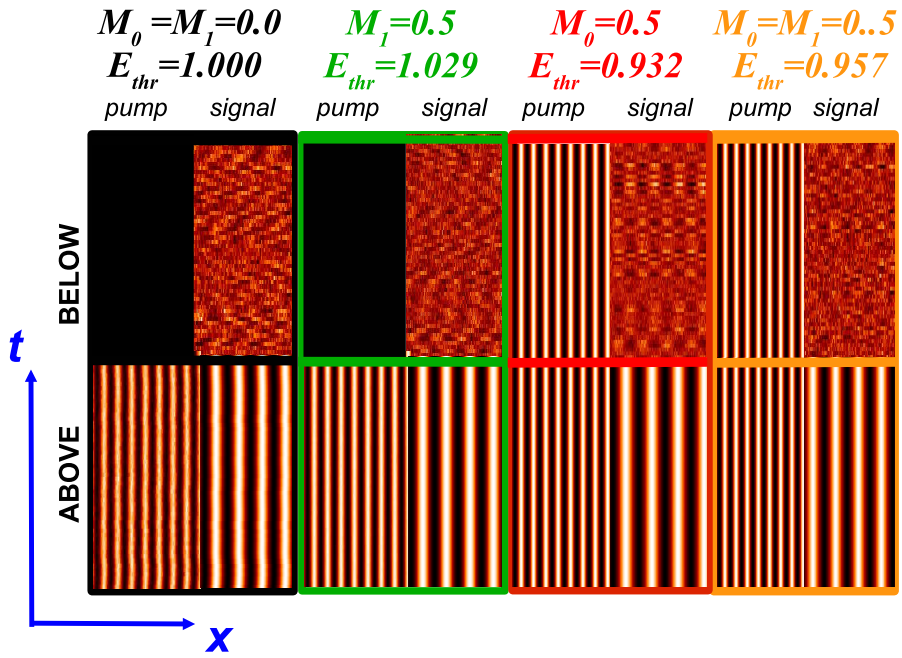

Figure 4.1. Near field of pump and signal field below and above the corresponding threshold for the case without photonic crystal and for different configuration of the photonic crystal ($M_0, M_1 = \{0.0, 0.5\}$). Simulations are performed 1% below (uppest row) and 1% above (lowest row) the corresponding threshold.

two intensities [Zambrini & al. (03)]

$$V_i(k) = \frac{\langle : [\hat{N}_i(k) - \hat{N}_i(-k)]^2 : \rangle}{S.N.(\hat{N}_i)} \quad i = 0, 1 \tag{4.1}$$

normalized to the corresponding shot noise value $S.N.(\hat{N}_i)$ for each k. This value represents the level of fluctuations found in a coherent state and can be obtained by subtracting to an operator variances its value in normal ordering. For the variance $V_i(k)$ the shot noise is proportional to the average of the sum of the intensities of the two beams with wavevectors $\pm k$. Negative values of $V_i(k)$ indicate sub-Poissonian statistics (as we described in the introduction) for the intensity difference of the two beams at $\pm k$ [Zambrini & al. (02)]. This is actually also equivalent to Spatial Antibunching (see Eqs. 1.33, 1.33 and 1.35). For our system we have reflection symmetry in the far field, that is:

$$\langle \hat{N}_i(k) \rangle \equiv \langle \hat{N}_i(-k) \rangle \quad and \quad \langle \hat{N}_i^2(k) \rangle \equiv \langle \hat{N}_i^2(-k) \rangle. \tag{4.2}$$

By developing this equation in Eq. 4.1, we obtain:

$$V_i(k) = 2\langle : \hat{N}_i^2(k) : \rangle - 2\langle : \hat{N}_i(k)\hat{N}_i(-k) : \rangle. \tag{4.3}$$

Remembering the spatial second-order coherent function and the spatial antibunching condition Eq. 1.35:

$$\langle : \hat{N}_i(k)\hat{N}_i(-k) : \rangle > \langle \hat{N}_i(k)^2 \rangle \tag{4.4}$$

we can determine that there will be spatial antibunching in our system, PCOPO, when $V_i(k) < 0$.

Even if both the variance $V_i(k)$ and the shot noise are functions of k, in some cases the normalized quantity (4.1) is uniform. In a linear analytical treatment below threshold, for homogeneous pump and detunings, $V_i(k) = -0.5$, independently of the pump intensity and of the wave-vector [Gatti & al. (97)1, Zambrini & al. (02)]. In the following we study how this variance is modified by the presence of the photonic crystal. As our stochastic equations provide average of antinormal ordered quantities, we present the relations between the antinormal and normal ordered expression of interest here.

From antinormal to normal ordering

The operators averages obtained from our numerical analysis correspond to antinormal order because are associated with the Q representation (introduced in Section 1.4). This can be related to expectation values in normal ordering by resting the proper quantities. We consider, as an example, the normal ordered variance of the number operator $\hat{N}(k) = \hat{a}^\dagger(k)\hat{a}(k)$

$$\langle : \triangle^2 \hat{N}_i : \rangle = \langle : \hat{N}_i^2 : \rangle - \langle : \hat{N}_i : \rangle^2 = \langle \hat{a}_i^\dagger(k)\hat{a}_i^\dagger(k)\hat{a}_i(k)\hat{a}_i(k) \rangle - \langle \hat{a}_i^\dagger(k)\hat{a}_i(k) \rangle^2 \tag{4.5}$$

where we omit the index i, being the formulation equivalent for pump and signal fields operators. We write the commutator as:

$$C_{kk'} = [\hat{a}_i(k), \hat{a}_i^\dagger(k')] = c\delta(k - k'). \tag{4.6}$$

where c is equal to one, before of field scaling (2.25). Normal ($: \quad :$) and antinormal ($\vdots \; \vdots$) ordered quantities are related by:

$$: \hat{N}_i(k) : \equiv \hat{N}_i(k) = \vdots \hat{N}_i(k) \vdots - C_{kk} \tag{4.7}$$

$$: \triangle^2 \hat{N}_i := \vdots \triangle^2 \hat{N}_i \vdots - 2\langle \vdots \hat{N}_i \vdots \rangle C_{kk} + C_{kk}^2. \tag{4.8}$$

The shot noise when measuring the variances of $\hat{N}_i$ can also be expressed in terms of antinormally ordered operators giving:

$$S.N.(\hat{N}_i) = \langle \vdots \hat{N}_i \vdots \rangle C_{kk} - C_{kk}^2. \tag{4.9}$$

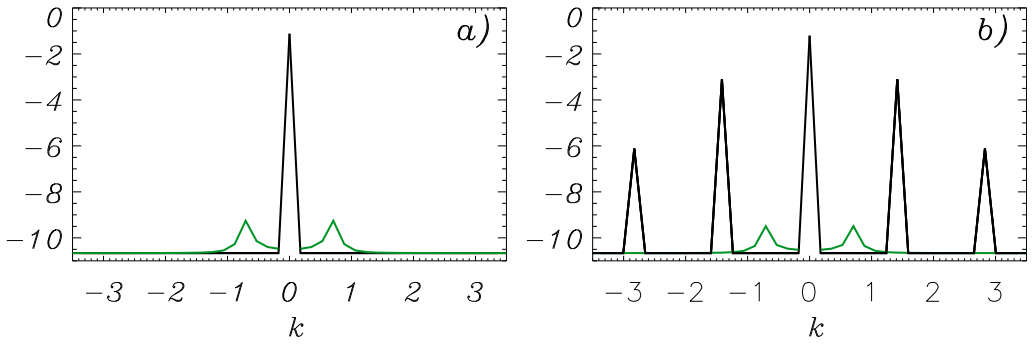

Figure 4.2. Logarithm of the pump (black) and signal (green) in the far field. Significant cases are represented, all of them 1% below the respective thresholds: a) $M_0 = M_1 = 0.0$ and $M_0 = 0.0$, $M_1 = 0.5$ (qualitative same result), b) $M_0 = 0.5$, $M_1 = 0.0$ and $M_0 = M_1 = 0.5$ (qualitative same result). The integration method used in the numerical simulation is described in previous papers [Zambrini & al. (00), Zambrini & al. (03), Bache & al.].

These relations are used to get normal ordered averages, like Eq. (4.1), from the antinormal ones obtained by numerical simulation of the stochastic spatio-temporal field dynamics in the Q representation. Notice that discretization in space due to numerical simulation needs to be taken into account in order to properly evaluate the commutator. Numerical results can indeed be compared with analytical expression when possible, as for the twin beams correlations in a OPO below threshold, without photonic crystal [Gatti & al. (97)1].

Numerical results

In the following we consider the PCOPO below threshold and with parameters:

$$\Delta_0 = 0; \quad \Delta_1 = -1; \quad k_{pc} = 2k_c \quad M_0, M_1 = \{0.0, 0.5\}. \tag{4.10}$$

We consider Eqs. 2.27,2.28 given in Chapter 2, with phase sensitive multiplicative noise $\xi_1(x,t)$ fulfilling 2.31,2.32 and 2.33 and numerically generated considering Eq. 2.30:

$$\xi_1(x,t) = \left[\frac{-\alpha_{0I}(x,t)}{2\sqrt{2+\alpha_{0R}(x,t)}} + \frac{i}{2}\sqrt{2+\alpha_{0R}(x,t)}\right]\phi(x,t) + \sqrt{\frac{1-\frac{|\alpha_0(x,t)|^2}{4}}{2+\alpha_{0R}(x,t)}}\psi(x,t)$$

[Zambrini & al. (03)], with $\alpha_0 = \alpha_{0R} + i\alpha_{0I}$ and ϕ, ψ uncorrelated real white noises in space and time, with variances one. In Fig. 4.2 we show the average far field intensities for the pump and the signal light fields, just below threshold, in three different cases. Pump modulation in this regime appears only when the pump detuning is modulated and, in this case, the even spatial harmonics of k_c are excited. Notice that, in absence of photonic crystals, these spatial modes would be intense only *above* threshold. The modulation of the photonic crystal has the wave-number of the spatial pattern that would

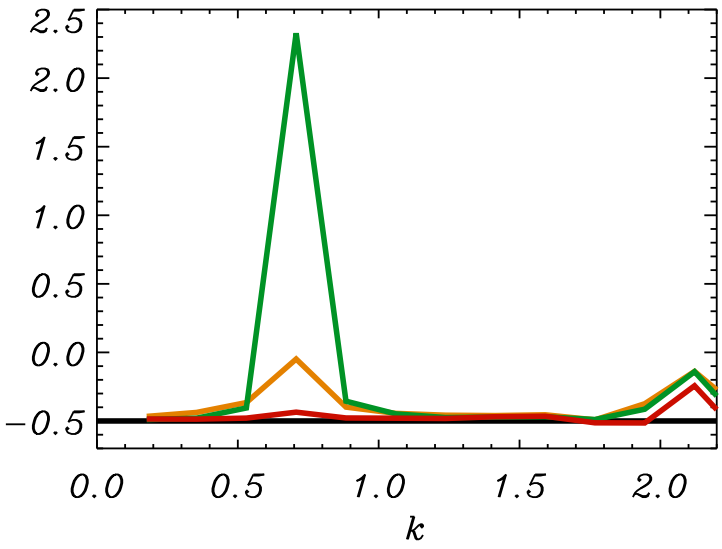

Figure 4.3. Normalized variance given by Eq.(4.1) 1% below the corresponding threshold for three different cases, like in Fig. 4.2: for $M_0 = M_1 = 0.5$ with $E = 0.95$ (orange), for $M_0 = 0.0$ and $M_1 = 0.5$ with $E = 1.02$ (green) and for $M_0 = 0.5$ and $M_1 = 0.0$ with $E = 0.93$ (red). The analytical value without photonic crystal yields the black line represented at -0.5 for $E = 0.99$. Quantum correlations correspond to negative values. We obtain significant loss of quantum correlations in $k_c = 0.7$ and $3k_c = 2.1$ for our choice of parameters.

arise above threshold, for an homogeneous OPO, $k_{pc} = 2k_c$. Other cases, $k_{pc} = nk_c$, are under investigation.

The average signal field vanishes because we consider pump values E just below threshold. As Fig. 4.2b show, however, modes with the critical wave-number ($k = k_c \simeq 0.7$ for our choice of parameters) are weakly damped and have a non vanishing average intensity. This is the regime of quantum images, extensively studied in the last decade and characterized by the 'spatial structures manifested by the correlation functions' between the field at different points, and also by 'noisy images' of the spatial fluctuations [Lugiato & al. (96)].

In the following, we consider twin beams correlations below threshold, where it is well known the analytical expression for the intensity correlations without photonic crystal, within linear approximation for the fluctuations dynamics [Gatti & al. (97)1, Zambrini & al. (03)]. In particular, the normalized variance Eq. (4.1) is homogeneous in k and is equal to -0.5 (black line in Fig. 4.3), as mentioned before. Any negative value of Eq. (4.1) corresponds to a non classical behavior. On the other hand, purely classical correlations appear in the pump. In particular, the average intensity of opposite modes $\pm k$ is the same (see symmetric plots in Fig. 4.2a), but the normal order variance vanishes, $V_0(k) = 0$ In Fig. 4.3 we represent the normalized variance $V_1(k)$ corresponding to the signal field, for the three cases discussed above, whose mean intensities are represented in Fig. 4.2b. The signal correlations are still non classical and around -0.5 for most of

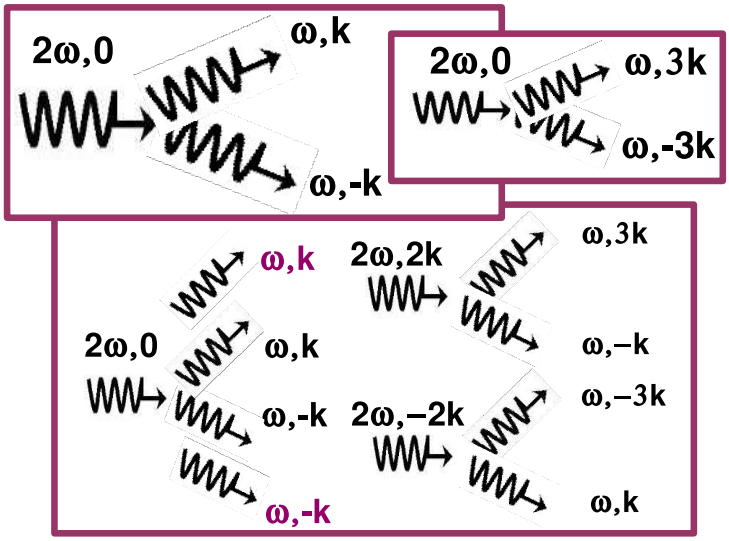

Figure 4.4. Primary Parametric Down Conversion processes are in the upper schemes, where $k = 0 \rightarrow k + (-k)$ is the most likely. Down, secondary processes as $2k \rightarrow 3k + (-k)$ and $2k \rightarrow (-3k) + k$ contribute to the correlations between opposite modes but their are not twin beams because they come from different depletions. Photons represented in magenta come from parallel primary processes. Such secondary processes are particularly relevant in the cases with modulation in the signal $M_1 \neq 0$ because photons at frequency ω are in the band gap so there are more incoherent deplected photons than twin ones (see Fig. 4.3).

the k values but they tend to deteriorate around critical points, namely k_c and $3k_c$. This can be interpreted in the following way. For $k_{pc} = 2k_c$, the photonic crystal favors the fluctuations in spatial harmonics in the fields, even below threshold. The presence of these modes is associated to secondary processes of photon creation and destruction [Zambrini & al. (02)]. These secondary processes, Fig. 4.4, give rise to the incoherent generation of photons with opposite wave-numbers and reduce the degree of correlation of photons generated in pairs. Interestingly, these correlations are quite robust crossing the instability threshold, and plots similar to Fig. 4.3 are found increasing the pump strength above the threshold for signal generation.

4.2 Translational Symmetry Breaking

For homogeneous detunings our system present translational symmetry in the transverse plane

$$x \rightarrow x + x_0 \tag{4.11}$$

for arbitrary values of x_0. In the presence of the intracavity photonic crystal the situation changes, because the transverse modulation of the refractive index represent a constraint

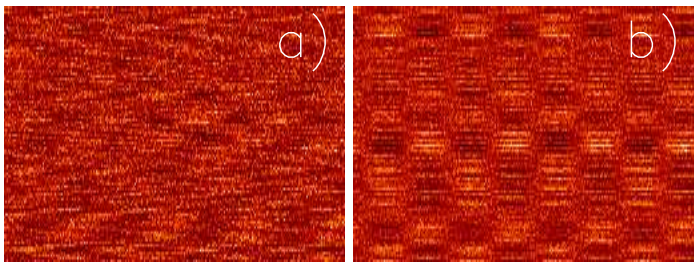

Figure 4.5. Spatio-temporal diagram of the near field quantum fluctuations in the real part of the signal field for parameters where the horizontal axis is x and the vertical one is time: a) $M_0 = M_1 = 0.0$, $k_{pc} = 2k_c$ and $E = 0.99$ like in Fig. 4.2a and b) $M_0 = 0.5$, $M_1 = 0$, $k_{pc} = 2k_c$ and $E = 0.923$ like in Fig. 4.2b.

that fixes the spatial origin. Then, the equations of the fields are not invariant under translations anymore. Above threshold this gives rise to a lock of the pattern position with respect to the photonic crystal. In some cases this translational symmetry break is also observed below threshold. In Fig. 4.5a we show the case without photonic crystal and in 4.5b is represented the case with $M_0 = 0.5, M_1 = 0.0$. Diffuse spatial structures are formed even below threshold, called *noisy precursors*, whose most intense spatial components can be seen in Fig. 4.2 (green lines). Such wave vectors are the least damped and they will be the selected in the spontaneous pattern formation above threshold. Without photonic crystals, these noisy precursors fluctuate in position 4.5a, while with photonic crystal, in some cases, they stand still 4.5b. Moreover, in Fig. 4.5b there are two different weakly damped modes that are in anti-phase. When increasing time in a fixed location (i.e. vertical line in 4.5b) we see that light and dark points are alternated within the stripe structure that can be recognized. Breaking of the translational symmetry is a fundamental property of the new modulated system with respect to OPO without photonic crystals and in the following we will study this effect through the variance of the transverse momentum.

4.2.1 Poynting Vector variance

Systems displaying translational symmetry are known to conserve linear momentum. We remind that, in optics, the momentum is proportional to the Poynting vector $\vec{S}$ [Hecht]. In order to characterize this translational symmetry breaking we numerically calculate the *transverse* momentum

$$\hat{S}_\perp = \int dk k (\hat{N}_0(k) + \hat{N}_1(k)). \tag{4.12}$$

In the case without photonic crystal and below threshold, the average transverse momentum does vanish, $\langle \hat{S}_\perp \rangle = 0$, because of the symmetric generation of photons with opposite momentum. Here we will focus in the momentum variance.

PUMP	$M_0 = M_1 = 0.0$	$M_0 = 0.5\ M_1 = 0.0$	$M_0 = 0.0\ M_1 = 0.5$	$M_0 = M_1 = 0.5$
E=0.9	-0.49	0.00	-0.36	0.00
E=1.1	-0.49	-0.32	-2.9	-0.14
$\sim 1\%$ *below thr*	-0.49	0.00	1.78	0.00
$\sim 1\%$ *above thr*	-0.49	-0.06	9.51	-0.04

Table 4.1. Numerical results for the variance of the Poynting vector, proportional to the linear momentum. In the case without photonic crystal (first results column) the values reproduce the result $V = -0.5$ given in [Gatti & al. (97)1] below threshold (even analytically) and in [Zambrini & al. (03)] above. When introducing the photonic crystal in its different configurations, we observe the momentum it is not constant anymore.

For the few modes cases, where only few intense modes contribute, the transverse Poynting vector can be approximated

$$S_\perp \approx k_c(\hat{N}_1(k_c) - \hat{N}_1(-k_c)) + 0\hat{N}_0(0). \tag{4.13}$$

The normally ordered variance of $S_\perp$ is proportional to the variance of the twin beams correlations (see Eq. 4.1):

$$\langle : \Delta^2 S_\perp : \rangle \propto V_1(k_c) \propto \langle : [\hat{N}_1(k_c) - \hat{N}_1(-k_c)]^2 : \rangle \tag{4.14}$$

As we reported in the previous section the degenerate OPO without photonic crystal below threshold allows for analytical solution, giving $V_1 = -0.5$, and the same value holds above threshold as was numerically calculated in [Zambrini & al. (03)]. It is interesting to prove that the momentum is not conserved when introducing the photonic crystal, by calculating the variance of the Poynting vector for the different configurations of the photonic crystal. Outcomes obtained in the calculations of the total transverse momentum variance, for different values of pump and photonic crystal transverse modulations, suggest that the linear momentum in the PCOPO is not longer preserved, indeed it is more noisy, see Tab.4.2.1.

4.3 Quadrature Squeezing

As it was presented in the introduction, it is possible to reduce the fluctuations of one quadrature field below the vacuum level, called shot noise. This is the squeezing phenomenon. Normal ordering allows us to immediately identify non classical features asso-

ciated with squeezing, as these lead to negative variances for the quadrature

$$\hat{X}(\theta) = \hat{a}e^{-i\theta} + \hat{a}^{\dagger}e^{i\theta} \tag{4.15}$$

which it is said to be squeezed in the interval given by Eq. 1.85:

$$-0.5 \leq \langle : (\Delta\hat{X}(\theta))^2 : \rangle < 0. \tag{4.16}$$

Hereby we are interested in the quadrature of the opposite signal modes superposition, defined as:

$$\hat{X}_{\theta,\phi}(k,-k) = (\hat{A}_1(k) + \hat{A}_1(-k)e^{-i\phi})e^{i\theta} + h.c. \tag{4.17}$$

In OPOs without photonic crystal, the values $\theta = 0$ and $\phi = 0$ give noise amplification, while fluctuations are damped for $\theta = 0$ and $\phi = \pi$, [Zambrini & al. (03)]. The quadrature variance at the critical wave number $\hat{X}_{\theta,\phi}(k_c,-k_c)$ reaches the minimum value just at threshold

$$\langle : (\Delta\hat{X}_{0,\pi})^2(k_c,-k_c) : \rangle = -0.5. \tag{4.18}$$

In this work we characterize this variance as a function of the superposition angle ϕ and the quadrature phase θ. The normal ordered variance is expressed in terms of the antinormally ordered correlations

$$\begin{aligned}\langle : (\Delta\hat{X}_{\theta,\phi})^2(k,-k) : \rangle = 2Re(\langle\hat{A}_1^2(k)\rangle e^{2i\theta}) + 2\langle\hat{A}(k)\hat{A}^{\dagger}(k)\rangle + \\ +2Re(\langle\hat{A}_1^2(-k)\rangle e^{2i(\theta+\phi)}) + 2\langle\hat{A}(-k)\hat{A}^{\dagger}(-k)\rangle + \\ +4Re(\langle\hat{A}_1(k)\hat{A}_1(-k)\rangle e^{i(2\theta+\phi)}) + 4Re(\langle\hat{A}_1^{\dagger}(k)\hat{A}_1(-k)\rangle e^{i\phi}) - 4C_{k,-k}\end{aligned}$$

where first order moments are neglected because they are vanishing below threshold. Remember that we simulate the equations 2.27, 2.28, in the Q representation, giving antinormal ordered moments, as explained in Chapter 2 and $C_{k,-k}$ is the commutator as in Section 4.1. In Fig. 4.6 the quadrature variance is represented for $k = k_c$ for the case without photonic crystal and for different configurations of the photonic crystal. In order to analyze the minimum and the maximum of the quadratures superposition variance we represent $\langle : (\Delta\hat{X}_{\theta,\phi})^2(\omega,k_c,-k_c) : \rangle$ as a function of θ for the value of ϕ that minimizes the variances, Fig. 4.7a. Below threshold and in absence of photonic crystal there is maximum squeezing. Due to the presence of the photonic crystal the correspondent variance increases as can be seen comparing black and colored curves in Fig. 4.7b.

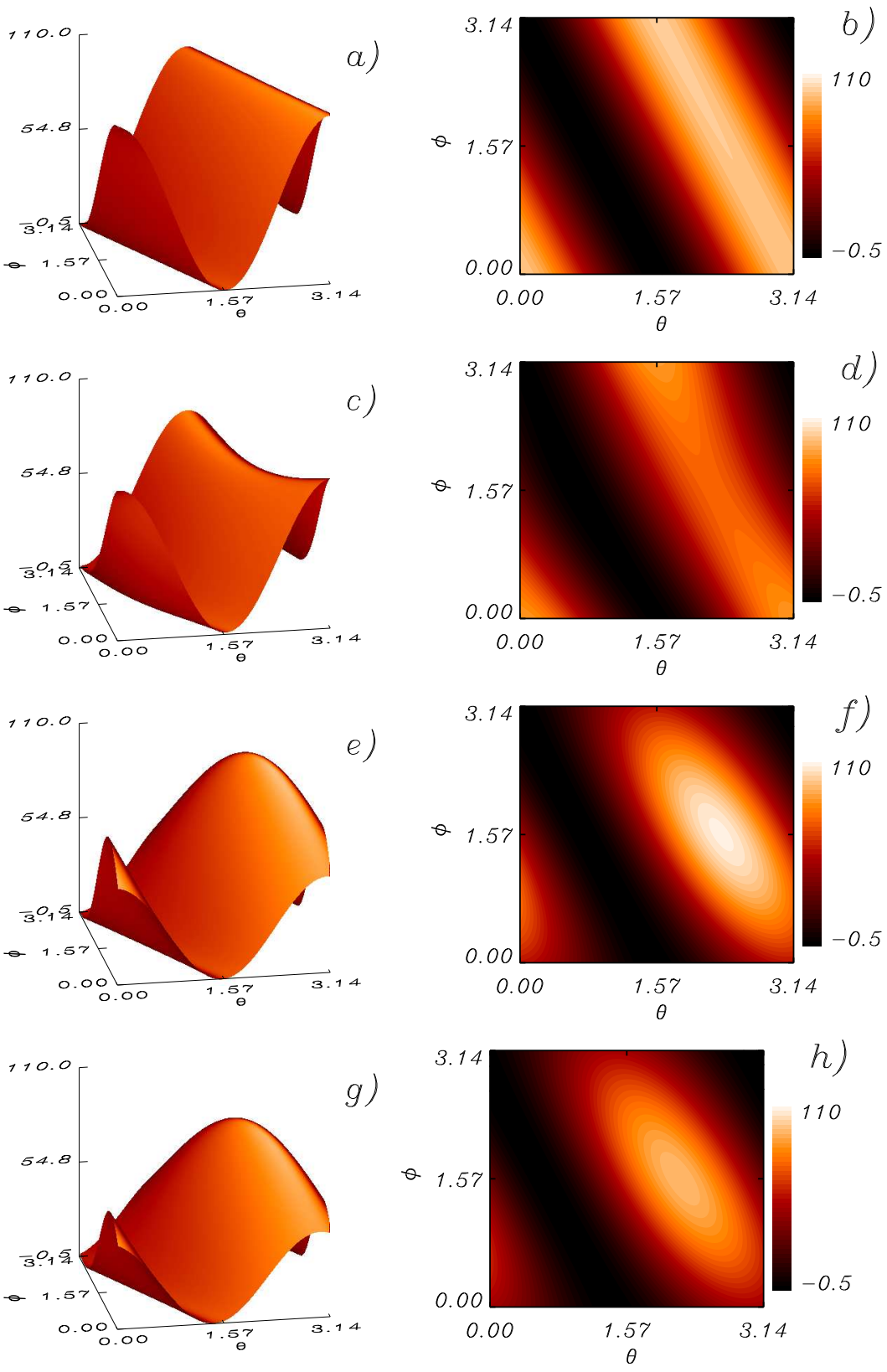

Figure 4.6. Variance of the quadrature for value of the superposition angle ϕ and the total phase θ for different configurations of the photonic crystal 1% below the corresponding threshold. a) and b) without photonic crystal; c) and d) with $M_0 = 0$ and $M_1 = 0.5$;

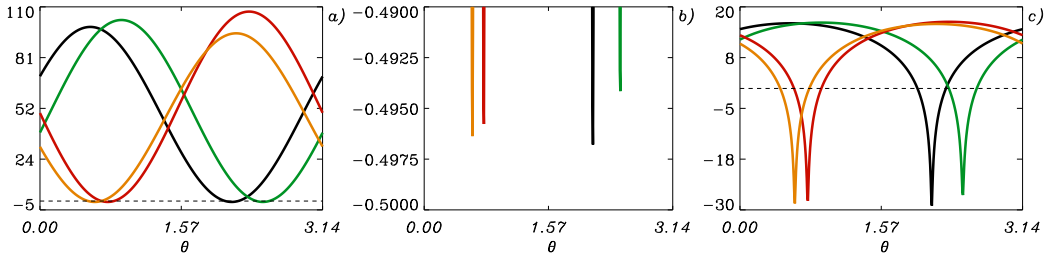

Figure 4.7. a) Variance of the quadrature $\hat{X}_{\theta\phi}(k_c, -k_c)$ in as a function of the total phase θ with the superposition angle ϕ where the variance reaches its minimum for different configurations of the photonic crystal 1% below the corresponding threshold. As usual, the amplitude of the modulations of the refractive index are, in black for the homogeneous case, i.e. $M_0 = M_1 = 0$, in green for $M_0 = 0, M_1 = 0.5$, in red for $M_0 = 0.5, M_1 = 0.0$ and in orange $M_0 = M_1 = 0.5$. The classical level is plotted in dashed line. b) Zoom at the minim values. c) Same in dB scale.

4.4 Summary

We are interested in how the photonic crystals act on the quantum phenomena taking place in OPOs. Firstly, by calculating the twin beam correlations variance $V_1(k)$, we have analyzed the Spatial Antibunching effect. We found that the presence of the intracavity photonic crystal modifies the twin beams correlations below threshold, generally degrading them. The most robust quantum correlations appear in the case in which the photonic crystal is only influencing the pump (red curve in Fig. 4.3). The lost of quantum correlations between most intense modes (signal at k_c and $3k_c$) is due to secondary processes. Modes with few photons preserve their quantum correlations (plateau at -0.5 in Fig. 4.3).

Below threshold we have shown noisy structures, called noisy precursors, and their change due to the transverse translational symmetry break (spatial locking of the noise pattern). Calculations are in progress in order to characterize this symmetry breaking in terms of the transverse linear momentum.

Finally, we have calculated the quadrature variance in PCOPO below threshold, drawing the conclusion that -at the same distance from the threshold- the squeezing generally decreases with respect to the case without photonic crystal. We advance that preliminary results above threshold show a positive effect of the use of photonic crystals.

5

Conclusions and Outlook

Interaction between light and matter allows to transform coherent laser states in non-classical ones, showing squeezing and entanglement. In particular, non-linear optical cavities as Optical Parametric Oscillators emit light with non-classical correlations between opposite Fourier spatial modes (twin beams). We considered here a PCOPO, that is an OPO in presence of an intracavity Photonic Crystal, described by a spatial modulation of the refractive index.
The introduction of photonic crystals in OPOs allows to control not only the instabilities of these devices but also its quantum fluctuations.
We have shown some preliminary results on the PCOPO below threshold. In general, we find that the spatial modulation of the detuning influences the spatial profile of the intensity fluctuations. Our main findings are that: (i) thresholds are raised or reduced by the photonic crystal depending on modulation strength; (ii) twin beams correlations showing antibunching persist below threshold but can deteriorate in correspondence of some wave-vectors, due to the incoherent excitation of secondary processes; (iii) squeezing below threshold is worsened in presence of photonic crystal.

In spite of the reported negative effect of the photonic crystal for squeezing, preliminary results of the squeezing *above* threshold show the possibility to actually increase the phase ranges for squeezing in PCOPO with respect to OPO, see Fig.5.1. The physical reason for this phenomenon can be attributed to the translational symmetry breaking due to the modulation of the space the photonic crystal creates, as we evaluated through the Poynting vector variance. This is the main part of this work and is in progress.
Moreover, new configurations, varying the spatial periodicity and strength of the photonic crystal, are under study, both from the classical (instability thresholds) and quantum

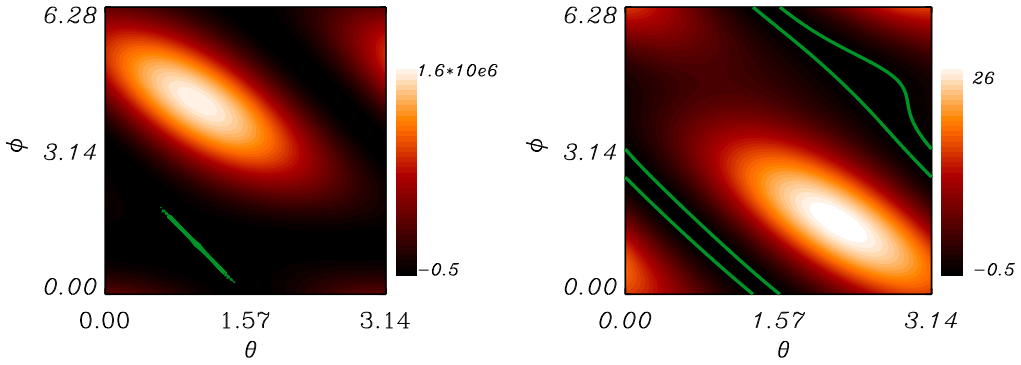

Figure 5.1. Normalized variance of the quadrature $\hat{X}_{\theta\phi}(k_c, -k_c)$ as a function of the quadrature angle θ and the superposition angle ϕ, on the left is the case without photonic crystal $M_0 = M_1 = 0$ and on the right the case in which the photonic crystal is affecting both pump and signal $M_0 = M_1 = 0.5$, 2% above the corresponding threshold. The darkest regions show quadrature squeezing, limited by the shot noise level in green. We see how photonic crystal allows to widen the squeezed quadrature range without worsening the degree of squeezing.

(non-classical correlations) points of view.

From one side, our objective is a general description of instability and creation of multistability offered by photonic crystals. On the other side, we plan to characterize the effect of the photonic crystal on squeezing and *EPR entanglement* from below to above threshold.

Bibliography

[Bache & al.] M. Bache, P. Scotto, R. Zambrini, M. San Miguel and M. Saffman, Phys. Rev. A **66**, 013809 (2002).

[Bachor & Ralph] H.S. Bachor and T.C. Ralph. *A guide of experimens in Quantum Optics*. Wiley (2004)

[Ball] P. Ball. *The self-made tapestry. Pattern formation in nature*. Oxford University Press (1999).

[Blanco & al.] A. Blanco, E. Chomski, S. Grabtchak, M. Ibisate, S. John, S. W. Leonard, C. Lopez, F. Meseguer, H. Miguez, J. P. Mondia1, G. A. Ozin, O. Toader and H.M. van Driel. Nature, **405**, 437-440 (2000)

[Boitier & al.] F. Boitier , A. Godard , E. Rosencher and C. Fabre Nature Physics, **5**, 267-270 (2009)

[Born & Wolf] M. Born and E. Wolf, *Principle of Optics* (Pergamon, Oxford, 1975).

[Boyd] R.W. Boyd, *Nonlinear Optics*, Academic Press, San Diego (1992).

[Brazhnyi] Brazhnyi, V.A. and Konotop, V.V. and Coulibaly, S. and Taki M. CHAOS, **17**, 037111 (2007)

[Burnham & Weinberg] D. C. Burnham and D. L. Weinberg, Phys. Rev. Lett. **25**, 84 (1970).

[Cahill & Glauber] K. E. Cahill and R. J. Glauber, Phys. Rev. 177, 1857 (1969); Phys. Rev. 177, 1882 (1969).

[Carmichael] H. Carmichael, *An Open Systems Approach to Quantum Optics*, Lecture Notes in Physics, Vol. **m18**, (Springer,Berlin, 1993).

[Collett & Gardiner] M.J. Collett and C.W. Gardiner, Phys. Rev. A **30**, 1386 (1984).

[Cross & Hohenberg] M. C. Cross and P. C. Hohenberg, Rev. Mod. Phys. **65**, 851 (1993).

[Einstein & al.] A. Einstein, B. Podolsky, and N. Rosen, Phys. Rev. **47**, 777 (1935).

[Franken & al.] P. A. Franken, A. E. Hill, C. W. Peters, and G. Weinreich, Phys. Rev. Lett. **7**, 118 (1961).

[Gardiner] C. W. Gardiner, *Handbook of Stochastic Processes* (Springer-Verlag, Berlin, 1985).

[Gatti & al. (97)1] A. Gatti, H. Wiedemann, L. A. Lugiato,

[Gerry] C. C. Gerry and P. L. Knight, *Introductory Quantum Optics*, Cambridge University Press (Cambridge, UK, 2005).

[Giovannetti & al] V. Giovannetti, S. Lloyd and L. Maccone. Science, **306** no. 5700, 1330 - 1336 (2004)

[Goda] K. Goda, O. Miyakawa, E. E. Mikhailov , S. Saraf , R. Adhikari , K. Mckenzie, R. Ward , S. Vass , A. J. Weinstein and N. Mavalvala. Nature Physics **4** 472-475 (2008)

[Gomila & Colet] D. Gomila, and P. Colet, Phys. Rev. E **66**, 046223 (2002).

[Gomila & al. (01)] D. Gomila, P. Colet, M. San Miguel and G.-L. Oppo, Phys. Rev. Lett **87**, 194101 (2001).

[Gomila & al. (02)] D. Gomila, P. Colet, M. San Miguel, A. Scroggie and G.-L. Oppo, IEEE J. Quantum Elect. **29**, 238 (2003).

[Gomila & al. (03)] Gomila, Damia and Zambrini, Roberta and Oppo, Gian-Luca. "Photonic Band-Gap Inhibition of Modulation Instabiblities", Phys. Rev. Letters, **92** (2004)

[Gomila & al. (04)] Damiá Gomila and Gian-Luca Oppo, Phis. Rev. E **72**, 016614 (2005)

[Graham] R. Graham, Phys. Rev. Lett. **52**, 117 (1984).

[Grynberg & al.] G. Grynberg, E. Le Bihan, P. Verkerk, P. Simoneau, J. R. R. Leite, D. Bloch, S. Le Boiteux, and M. Ducloy, Opt. Commun. **67**, 363 (1988).

[Grynberg & Lugiato] G. Grynberg and L. A. Lugiato, Opt. Commun. **101**, 69 (1993).

[Hanbury Brown & Twiss] R. Hanbury Brown and R. Q. Twiss, Nature (London) 177, **27** (1956).

[Hecht] E. Hecht, Am. J. of Phys. **38**, 1156 (1970).

[Huang] K. Huang, *Statistical mechanics*, 2nd ed. (John Wiley & Sons, New York, 1987)

[Joannopoulos & al.] J. D. Joannopoulos, S.G. Johnson, J. N. Winn and R. D. Meade. *Photonic Crystals. Molding the Flow of Light.* 2 edition, Princeton University Press (2008)

[John] S. John. Phys. Rev. Lett. **58** 24862489 (1987)

[Kimble & al.] H. J. Kimble, M. Dagenais and L. Mandel, Phys. Rev. Lett**39**, 691 (1977).

[Kolobov] M. I. Kolobov, Rev. Mod. Phys., **71**, 1539 (1999).

[Khurgin] Khurgin, Jacob B. "Mirrorless magic", Nature Photonics, **1**,446-447 (2007)

[Canalias& Pasiskevicius] Interview to C. Canalias and V. Pasiskevicius. "Who needs mirrows?", Nature Photonics, **1**, 484 (2007)

[Lassen & al.] M. Lassen, P. Tidemand-Lichtenberg, and P. Buchhave, Phys. Rev. A **72**, 023817 (2005)

[Le Berre & al.(79)] M. Le Berre-Rousseau, E. Ressayre, and A. Tallet, Phys. Rev. Lett. **43**, 1314 (1979).

[Leuchs & al.] G. Leuchs, Ch. Silberhorn, F. König, A. Sizmann, and N. Korolkova: *Quantum solitons in optical fibres: basic requisites for experimental quantum communication*, in *Quantum Information Theory with Continuous Variables*, S.L. Braunstein and A.K. Pati eds. (Kluwer

Academic Publishers, Dodrecht 2002).

[Loudon] R. Loudon, *The quantum theory of light*, Clarendon Press (Oxford, 1983).

[Lugiato] *Special issue: Nonlinear Optical Structures, Pattern, Chaos*, in Chaos Solitons & Fractals **4**, no.8/9 (1994). Guest editor: L. A. Lugiato.

[Lugiato & al.] L. A. Lugiato, C. Oldano, Phys. Rev. A **52**, no. 2, 117-120 (1984)

[Lugiato & al. (95)] L. A. Lugiato, A. Gatti, and H. Wiedemann, *Quantum fluctuations and nonlinear optical patterns*, Les Houches, session LVIII, 1995, edited by S. Reynaud, E. Giacobino, and J. Zinn Justin (Elsevier-North-Holland, Amsterdam, 1997).

[Lugiato & al. (96)] L. A. Lugiato, S. M. Barnett, A. Gatti, I. Marzoli, G. L. Oppo, and H. Wiedemann, pg. 5, in *Coherence and Quantum Optics VII*, edited by Eberly, Mandel, and Wolf, Plenum Press (New York, 1996).

[Lugiato & al. (97)] L. A. Lugiato, A. Gatti, H. Ritsch, I. Marzoli, and G. L. Oppo, J. Mod. Opt. **44**, 1899 (1997).

[Lugiato & al. (99)] L. A. Lugiato, M. Brambilla, and A. Gatti, "Optical Pattern formation", in *Advances in Atomic Molecular and Optical Physics* **40**, 229, B. Bederson and H. Walther eds. (Academic Press, New York, 1999).

[Lugiato & al. (02)] L. A. Lugiato, A. Gatti, and M. Brambilla, J. Opt. B **4**, S1 (2002).

[Lugiato & Castelli] L.A. Lugiato and F. Castelli, Phys. Rev. Lett. **68**, 3284 (1992).

[Lugiato & Grynberg] L. A. Lugiato and G. Grynberg, Europhys. Lett. **29**, 675 (1995).

[Lugiato & Lefever] L. A. Lugiato and L. Lefever, Phys. Rev. Lett. **58**, 2209 (1987).

[McKeever & al.] J. McKeever, A. Boca, A. D. Boozer, J. R. Buck and H. J. Kimble Nature **425**, 268-271 (2003)

[Mandel & Wolf] L. Mandel and E. Wolf, *Optical coherence and quantum optics* (Cambridge University Press, Cambridge, 1995).

[Marsal & al.] N. Marsal, D. Wolfersberger, M. Sciamanna, G. Montemezzani and D. N. Neshev. Optics Letters **33**, 21 (2008)

[Nielsen & Chuang] M. A. Nielsen and I. L. Chuang, *Quantum Computation and Quantum Information* (Cambridge University Press, Cambridge, 2002).

[Noda & al] S. Noda, K. Tomoda, N. Yamamoto, A. Chutin. Science, **289**, no. 5479, 604-606, (2000)

[Nogueira & al.] W. A. T. Nogueira, S. P. Walborn, S. Pádua, and C. H. Monken, Phys. Rev. Lett. **86**, 4009 (2001); Phys. Rev. A **66**, 053810 (2002).

[Oppo & al. (94)] G-L. Oppo, M. Brambilla, L. A. Lugiato, Phys. Rev. A **49**, 2028 (1994); G.-L. Oppo, M. Brambilla, D. Camesasca, A. Gatti, and L.A. Lugiato, J. Mod. Opt. **41**, 1151 (1994).

[Pawula] R. F. Pawula, Phys. Rev. **162**, 186 (1967).

[Peckus & al.] Peckus M, Staliunas K, Nizauskaite Z, et al

[Sakurai] J. J. Sakurai, *Advanced Quantum Mechanics*, Addison-Wesley (1967), pag. 35.

[Schnabel] R. Schnabel. Nature Physics, **4** (2008)

[Slusher & al.] R. E. Slusher, L. W. Hollberg, B. Yurke,J. C. Mertz and J. F. Valley, Phys. Rev. Lett. **55**, 2489 (1985).

[Stoler] D. Stoler, Phys. Rev. D **1**, 3217 (1970); **4**, 1925 (1971).

[Sudarshan] E. C. G. Sudarshan, Phys. Rev. Lett. **10**, 277 (1963).

[Sun] H. Sun, S. Matsuo and H. Misawa. Appl. Phys. Lett. **74**, 786 (1999)

[Teich & Saleh] M. C. Teich and B. E. A. Saleh, *Photon bunching and antibunching*, Prog Opt. **26**, 1-104 (1988)

[Terhalle & al.] B. Terhalle, N. Radwell, P. Rose, C. Denz and T. Ackemann. Applied Physics Letters **93**, 151114 (2008).

[Vahlbruch & al.] H. Vahlbruch, M. Mehmet, S. Chelkowski, B. Hage, A. Franzen, N. Lastzka, S. Goβler, K. Danzmann and R. Schnabel. Phys. Rev. Lett. **100**, 033602 (2008)

[Walls & Milburn] D. F. Walls, G. J. Milburn, *Quantum optics*, Berlin (Springer, 1994).

[Yablonovitch (87)] E. Yablonovitch. Phys, Revi. Lett. **58**, 20592062 (1987).

[Yablonovitch (00)] E. Yablonovitch. Science, **289**. no. 5479, 557-559, (2000)

[Yuen] H. P. Yuen, Phys. Rev. A **13**, 2226 (1976).

[Zambrini & al. (00)] R. Zambrini, M. Hoyuelos, A. Gatti, P. Colet, L. Lugiato, and M. San Miguel. Phys. Rev. A **62**, 63801 (2000).

[Zambrini & al. (02)] R. Zambrini, S. M. Barnett, P. Colet, and M. San Miguel, Phys. Rev. A **65**, 023813 (2002).

[Zambrini & al. (03)] R. Zambrini, S. M. Barnett, P. Colet, and M. San Miguel, Eur. Phys. J. D **22**, 461 (2003).

[Zambrini] PhD thesis *Quantum Fluctuations in Non Linear Optical Systems*. R. Zambrini (2003)

[Zeilinger] A. Zeilinger. *The Physics of Quantum Information, Quantum Teleportation ans Quantum Cryptography*. Eds. Bawmaster, Ekert and Zeilinger. Springer (2000)